Decomposition of Supermassive Black Hole host galaxies in near-infrared

Master's Thesis
University of Turku
Dept. of Physics and Astronomy
Astronomy
2025
BSc Chantal Babooram
Reviewed by:
Dr. Kari Nilsson.
Prof. Jari Kotilainen.

The originality of this thesis has been checked in accordance with the University of Turku quality assurance system using Turnitin OriginalityCheck service.

UNIVERSITY OF TURKU
Department of Physics and Astronomy
BABOORAM, CHANTAL Thesis
Master's Thesis, 43 pages
Astronomy
December 2025
The originality of this thesis has been checked in accordance with the University of Turku quality assurance system using the Turnitin OriginalityCheck service

---

The co-evolution between black holes and galaxies is still poorly understood to this day. The black hole properties have been known to correlate with properties of their host galaxies. Over the years, there has been an increase in super massive black hole measurements, which leads to more detailed observational analysis and understanding of black holes and their evolution with their host galaxy. Using deep near infrared (NIR) imaging from the TNG telescope of a sample of black hole host galaxies, this thesis aims to produce galaxy decompositions into the bulge and disk components to further understand the Black hole mass and their host galaxy correlation. The NIR imaging provides the advantage of reducing effects of the dust obscuration. In this thesis we obtain sub-arcsecond resolution near-infrared data for 9 galaxies. Galaxy decomposition was performed on the data set, where the bulge parameter was obtained through the use of the program GALFIT. The data showed similar correlations to other papers, suggesting the black hole masses correlate with the host galaxy bulge luminosity.

Keywords: Galaxies, Black Holes, GALFIT, TNG telescope,

Contents

1 Introduction

Stellar mass black holes (BH) are formed from the gravitational collapse of a star. They are dense and the gravity in the region does not allow anything to escape, not even light. Super massive black holes (SMBH) are vastly larger than stellar black holes. Most SMBHs are assumed to be in the centers of galaxies and have masses $M_\bullet > 10^6 M_\odot$ [1]. Having such large masses raises the question of their formation.

Galaxies are fundamental in understanding the structure and evolution of the universe, as they were formed early in the universe′s history. They are gravitationally bound, containing stars, dust and interstellar gas and they come in various forms. The luminosity of a galaxy can be determined by the distance. The distances are also needed to estimate the masses of galaxies.

Galaxies were classified by Edwin Hubble based on their appearance into the Hubble Classification. This is shown in Figure 1, also known as the tuning fork diagram. There are four classifications; elliptical, normal spirals, barred spirals and irregulars. The elliptical galaxies are divided into subtypes E0, E1 to E7, where the integers are rounded up from 10(1-b/a), where a and b are semi major and semi minor axes, respectively. Spiral galaxies are separated into barred spiral and normal spiral, depending on if there is a bar like structure visible within the spiral arms of the galaxy.

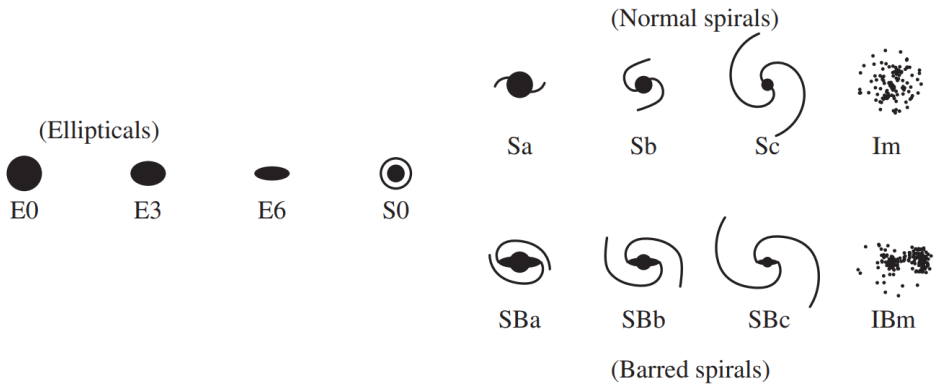

Figure 1. Hubble sequence diagram of the morphology of galaxies [2].

The luminosity of galaxies range from $10^{12}L$sun to $10^{13}L$sun. In elliptical galaxies, the stellar motions are random, and their mass can be estimated from the velocities of the stars and interstellar gas. This leads to the observed size of galaxies being an important constraint for galaxy formation models. Surface brightness profiles $I(R)$ are defined as the surface brightness of the isophotal semimajor axis (R) for elliptical galaxies. The surface brightness profiles of spheroid galaxies are fit well by the Sérsic profile, $R^{1/n}$ [3]. The isophotes are fitted by ellipses which are defined by the minor to major axis ratios $\frac{b}{a}$.

Decomposing disk galaxies into their components most often use the exponential profiles for the disk and a Sérsic profile for the bulge. In previous studies, [4] showed a relation between the black hole mass and spheroidal stellar mass of galaxies shown Figure 2. They also showed that bulges have more elliptical isophotes and late type disk galaxies have boxy isophotes.

It is important to understand the connection between supermassive black holes and their host galaxies to understand the role of galaxies in the history of structure formation [5]. It has been established that the stellar masses of host galaxy bulges are tightly correlated to their SMBH masses [1][5][6][7][8][9][10]. It was also found by [9][6][7][11] that there was a correlation between black hole masses and velocity

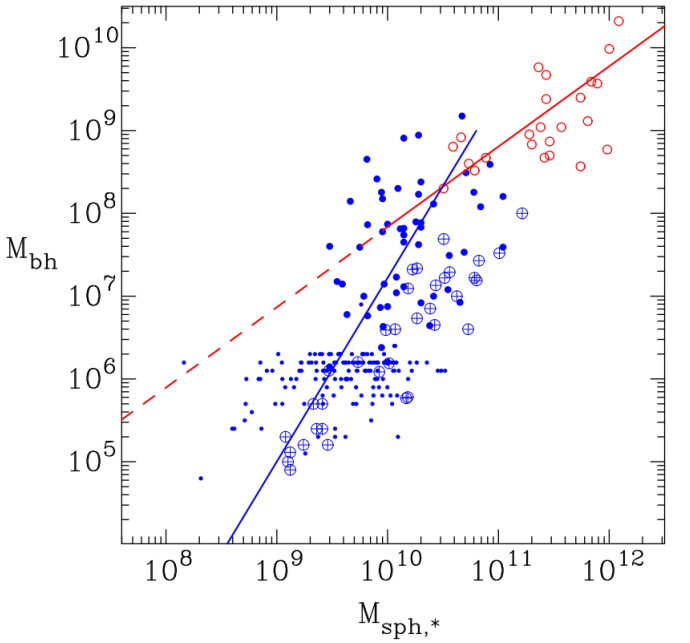

Figure 2. Plot shows Black Hole mass vs mass spheroid in a sample of galaxies. The Sérsic galaxies are shown by the filled blue circles and the core Sérsic galaxies are the open red circles. The red and blue lines show the near-linear and near-quadratic scaling relations, for core Sérsic and Sérsic galaxies, respectively [4].

dispersion of the host bulge. In the paper [7] such correlation was also found, suggesting a connection with the formation and evolution of the bulge and black holes.

Galaxies of stellar mass $M_\star \geq 10^9 M_\odot$ are assumed to have supermassive black holes of mass $M_\bullet \geq 10^{\,6}\, M_\odot$ at their centers [11]. Their large size leads to the question that they may have been formed by unexplained massive seeds in the early universe before galaxy formation or from angular momentum transfer to get them to their current sizes. The observational correlations were used to make a model of the joint BH-speroid formation, which explains these correlations and the Active Galactic Nuclei (AGN) feedback [12]. Detailed photometric analysis and dynamic models are required to further understand BH formation and SMBH galaxy coevolution. The data in this thesis will add to previous studies [13][14][15].The galaxies were all chosen to be early- type galaxies with sizes ranging $10^6 M_\odot$ to $10^9 M_\odot$ which continues

from a previous paper [13].

The correlation between the bulge mass and luminosity [1] suggest the co-evolution of BHs and bulges, where they regulate each others growth. Figure 3 shows such correlations for many galaxies.

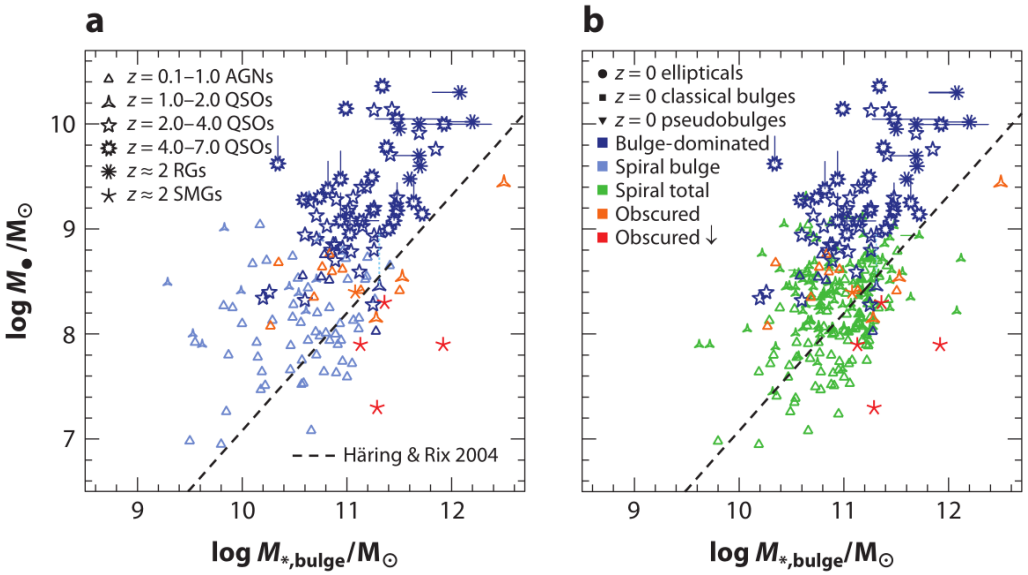

Figure 3. The plots show the correlation between M $_\bullet$ and M$_\star$ of AGNs that have a range of z $\sim$ 0.1 to 7.1. The bulge only is shown in and (a) for for the galaxy in (b). The dashed line from [8] is the same correlation bulge at z $\sim$ 0. Dark blue are either ellipticals, or classical bulges or large enough that they may be bulge dominated [1].

Many bulgeless galaxies have been found to have BHs with masses around 10^5 to 10^6Msolar [1]. This may mean that having a classical elliptical bulge galaxies is not necessary for BH formation, but even though they exist in galaxy disks their properties have not been found to correlate to those of galaxy disks [1].

While [1] have showed that the BH masses tightly correlate with elliptical and classical bulge galaxies, the correlation is weak with pseudobulge galaxies and dark halos, which does not imply any relationship. The only relation that has been implied, is that the BHs grow easily in bigger galaxies with more fuel. There is currently have no correlation with disk galaxies.

It was suggested by [1] that the galaxies and the SMBH evolve together but they do not have to influence each other. Weak coevolution is where the galaxy would

influence the growth of the BH, by controlling the feeding and merging. A strong form of coevolution would be that the BH may control the properties of the galaxy through energy and momentum feedback into the galaxy. In this study, black hole masses and their bulge magnitudes are looked at.

2 Data Acquisition and Reduction

2.1 Data Acquisition

The sample of galaxies for the thesis comes from a larger sample in [17]. The larger sample consisted of around 230 BHs which [17] used to explore the scaling relations between BHs and their host galaxy. Data for BHs in the parent sample with $\sim$24mag/arcsec^2 depth were only available for around 50 out of about 200 BH hosts. The targets chosen for this study adds to already existing data. Some of the smaller galaxies were chosen from the set that had an $R_e < 25''$, which were able to fit within the field of view of the TNG NICS telescope of $4'$ x $4'$. The seeing of FWHM of < 1 arcsec was necessary for the decomposition of the galaxy into their bulge and disc components. The exposure time was 300-315 seconds per target in the K-band, which was adequate to measure the galaxy profiles to $\sim$24mag/arcsec^2. Sky-offsets were obtained with the same exposure time and used to subtract the background flux. The exposure was broken up into 30 dithered, 20 second exposures on target.

The total amount of time per object was around 1500 seconds. The targets were above -30 degrees declination which made is possible to observe them above airmass of 2. For NIR images, moonlight did not affect and imaging and photometric sky conditions were not required. The Galaxies in the data set are shown in table 1.

Object	RA	DEC	Hubble Type	Distance (Mpc)	Black hole Mass($M_\odot$)	K-band Magnitude	Total Tme (sec)	Observation date
J0437+2456	04:37:03	56:06.00	S D	66.0±6.6	6.45±0.03	12.6	315	2017-12-03
NGC 5879	15:09:47	00:01.00	SA(rs)bc:?	10.6±1.1	$6.62^{+0.28}_{-6.62}$	11.2	315	2017-07-05
NGC 6086	16:12:36	29:05.00	E	138.0±11.5	9.57±0.17	11.6	315	2017-07-05
NGC 6500	17:55:60	20:18.00	SA ab	36.5±3.6	8.34±0.26	10.6	330	2017-07-05
UGC 12064	22:31:21	21:30.00	S0^-	34.7±6.7	8.84±0.52	11.1	300	2017-09-06
NGC 7332	22:37:25	47:54.00	S0	21.7±2.2	7.08±0.18	10.0	300	2017-09-06
NGC 7469	23:03:16	52:26.00	(R)SAB(rs)a	47.7±8.1	6.94±0.16	9.8	300	2017-09-06
IC 1481	23:19:25	54:22.00	S?	89.9±9.0	7.15±0.13	12.2	300	2017-09-06
NGC 7682	23:29:04	32:00.00	SB(r)ab	59.3±5.9	7.56±0.33	12.2	300	2017-09-06

Table 1. The table shows the targets, Hubble type, distance, black hole mass, date and exposure times and the K-band magnitude. The magnitudes were found using NASA/IPAC Extragalactic Database, the black hole masses are taken from[17] and the Hubble types are from [18].

2.2 Data Reduction

The images were reduced and co-added with sky subtraction first before using GALFIT to perform two-dimensional galaxy decomposition. The data reduction process was done using, Image Reduction and Analysis Facility (IRAF). Sky images had to be first created before subtracting them from each image. The images were first grouped into sets of four, where for each set a separate sky image was produced. This was done by using **imcombine** in each image. The sky image was then subtracted using **imarith** from each image in the set. This process was repeated for each set. An example of the data reduction process can be seen in figure 4.

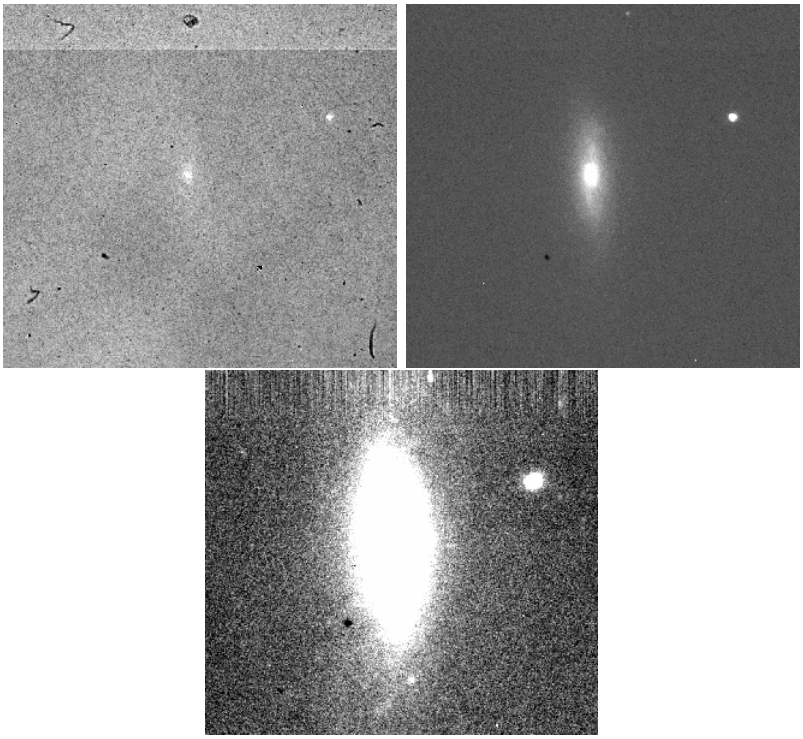

Figure 4. The top left image shows the original image. The top right shows one sky subtracted image.The bottom image shows the combined sky subtracted images used for GALFIT.

The coordinates for the target in each image were obtained using **imexamine**. Coordinate files with the galaxy position and the new position that was at the center of the image were made. The new position for the target was often near the center

of the image or there was an image where the target was already at the center. The list of coordinates was then used in **geomap** to obtain the transformation from the original coordinates to the new coordinates in a database, that would then be used to shift all the targets to the new position. A script was then made to move each image by the correct xy amount. The images were then combined using **imsum**.

3 Surface brightness modeling

3.1 Introduction to GALFIT

GALFIT[1] is a two-dimensional fitting program, that uses analytic functions to extract the structural components of observed images [19]. GALFIT improves on previous fitting algorithms, allowing for more accurate 2D models of the light distribution for galaxies. The program can model point sources, elliptical galaxies and spiral arms to name a few. Version 3 of GALFIT was used to analyze the bulge and disk luminosities for the data. After GALFIT was installed, it was tested using the example file provided to ensure it worked properly.

The example contained a template input file, that showed the relevant parameters for the provided galaxy. An example of the input file can be seen in the appendix. Detailed information on the components and parameters can be found in the GALFIT manual [20]. The input file is used to list the relevant components that would be fitted. Each component has a set of free parameters to initially set, such as: position, integrated magnitude, Sérsic index, axis ratio and position angle. The first section in the input file contains a set of parameters to set. Some of the items in the first section are image name, output name, PSF image, plate scale and fitting region. The second section is where the object fitting parameters are set. Each components has three columns for information. The first column contains the initial values for the parameters in the given component. The second column is used to indicate if a parameter is left free or fixed. If the value was set to 1 they the parameter would be varied. If it was set to 0 they the parameter was not varied. Setting some parameters to 0, can be useful when a value does not converge at an optimal value. The third column contains the description for the parameter.

[1] https://users.obs.carnegiescience.edu/peng/work/galfit/galfit.html

GALFIT is run from the terminal with the line:

galfit galfit.feedme,

where galfit.feedme would be the name of the input file. GALFIT requires all the files that are needed to begin the fit to be in the same folder. The program tries to minimize χ^2, which is defined by the Equation (1) [19].

$$\chi^2_\nu = \frac{1}{N_{\mathrm{DOF}}} \sum_{x=1}^{nx} \sum_{y=1}^{ny} \frac{\left(f_{\mathrm{data}}(x,y) - f_{\mathrm{model}}(x,y)\right)^2}{\sigma(x,y)^2} \tag{1}$$

GALFIT calculates the χ^2 value and then uses the value to adjust the parameters for each next step. This continues until the minimum chi squared if found. The equation shows that GALFIT requires the input data $f_{\mathrm{data}}(x,y)$ and the sigma image $\sigma(x,y)^2$. GALFIT generates a sigma value based on Poisson statistics for the data image. The $f_{\mathrm{model}}(x,y)$ model image is also internally generated as it tries to find the best match for the given data. The value of N_{DOF} is the number of degrees of freedom which is approximately nx x ny, where they are the x and y dimensions of the image, respectively.

The program outputs three files after it runs. The fit.log file contains the final values and errors and each new pass of GALFIT is appended to the log file. The second file galfit.NN, where NN is the value that keeps increasing with every fit, includes all the parameters and the final values. The last file that is output is the image block fits file. Within the data block contains four slices. The zeroth slice is always a blank image. The first slice is the original image. The model created by GALFIT is on the second slice. The residual image made by subtracting the model from the original image which is seen on the third.

3.2 Preparation files for GALFIT

3.2.1 PSF Construction

Several files needed to be prepared before running GALFIT. The PSF image, the bad pixel mask and the image of the galaxy. The PSF image size was chosen to be around 20×20 pixels depending on the size of the star. This was done to avoid contaminants from stars in crowded fields. A PSF image was made for each galaxy using the IRAF **daophot**, **pstsel** and **psf** tasks[2]. More than one star was used when the flux of the stars in the image were low. Choosing relevant stars required following strict criteria. Stars where the peak was too low such as < 500 ADU′s, or if they were too bright (> 12000 ADU′s) were not used to make the PSF image. Stars that were crowded in the 20×20 pixel box were also excluded. Double stars or galaxies were also excluded from the choices. The stars chosen had to be approximately circular with a large flux.

Once the stars were selected, the brightest pixel was acquired using IRAF **imexamine**. GALFIT requires that the PSF should have the peak flux at the very center for accurate convolution. Several galaxies only required one star as a PSF image, as the star had a high enough flux for convolution. Low flux stars caused the convolution to be incorrect during the fitting process or to cause the program to crash. Stars with approximately > 5000 ADU′s gave considerably better results with convolution. An example of a radial plot that was chosen for a PSF image is shown in figure 5.

[2]https://users.utu.fi/kani/opetus/psfohje/PSF.html

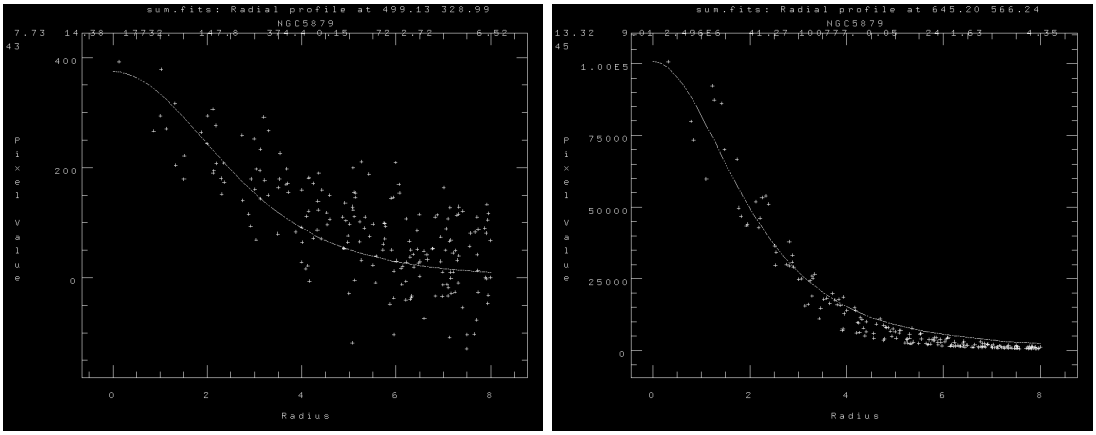

Figure 5. The left image shows a radial plot of a star that was not adequate for a PSF image. The right image shows a radial plot of a star that had a high enough ADU count for a PSF image.

3.2.2 Bad Pixel Mask

The bad pixel mask was created using IRAF. Using **imarith**, a copy of the galaxy image was made where all the pixel values were 1. The task **imedit** was then used by setting a round aperture, a pixel value of 0 and a pixel radius large enough to cover the galaxy. The images that were made were checked after creation to ensure that only the galaxy was completely revealed. Any further creation that included extra stars, was edited by re-masking stars with a pixel value of 1.

3.3 Sérsic and Disc Profiles

The Sérsic powerlaw is used in studying galaxy morphology, where it is common for fitting one component on galaxies. It is represented by Equation (2).

$$\Sigma(r) = \Sigma_e exp\left[-\kappa\left(\left(\frac{R}{r_e}\right)^{1/n} - 1\right)\right] \tag{2}$$

In Equation (2) Σ_e is the pixel surface brightness with effective radius r_e, n is the concentration parameter, where the galaxy has a steep inner profile when n is large and a shallow inner profile when n is small. Half of the galaxy′s flux is contained

within an ellipse of r_e. A Sérsic profile where n=4 is called a de Vaucouleurs profile. The Sérsic profile can be seen in figure 6. The exponential profile is the Sérsic profile where n=1.

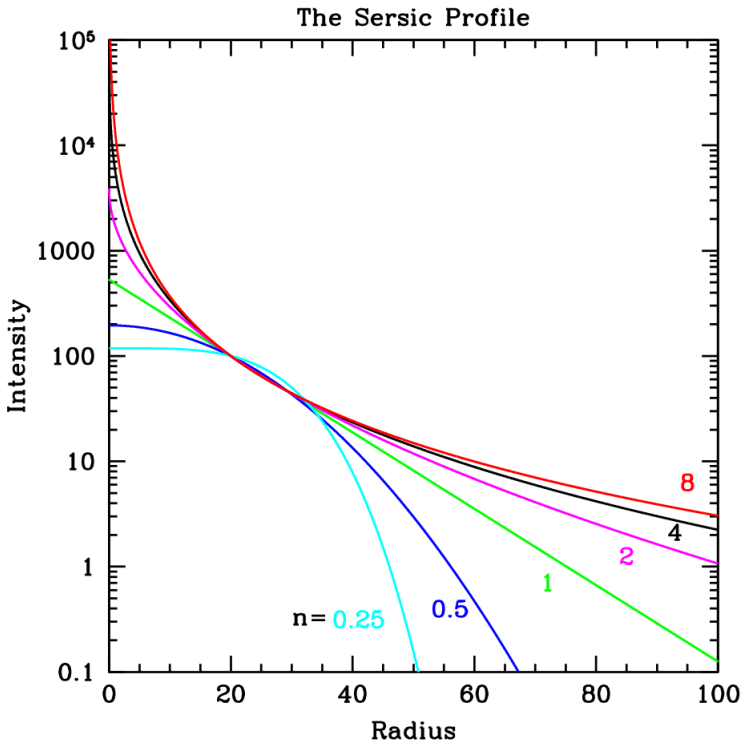

Figure 6. Examples of the Sérsic profile. When n is larger the profile is steeper at the core, where when n is small and the profile is flatter at the core. Special cases of Sérsic profile are: The exponential disk profile is where n=1 and n=4 for the de Vaucouleurs profile [19].

The exponential disc is used on disc galaxies. The equation has the form

$$r_e = 1.678 r_s (\text{for n} = 1 \text{ only}) \tag{3}$$

$$\Sigma(r) = \Sigma_0 exp\left(-\frac{r}{r_s}\right) \tag{4}$$

The equation has the form where r_s is the scale length of the exponential disc. An AGN component was added to some galaxies to help produce a better fit although

not all galaxies had an AGN component.

3.4 GALFIT analysis

Several galaxies were left out of the reductions and analysis due to having too few images to work with. The data set for J0437+2456 had enough images taken by the telescope to produce a combined image to analyze, but the galaxy was too faint for it to be combined into an image which was suitable for further analysis with GALFIT. Bulge and disc components were only used in this study as more complex components were not possible. Some galaxies had a bright center and a PSF component was added. The positions for the galaxy were found using **imexamine**, which was then used for the GALFIT parameters. These were held fixed for both bulge as disc to avoid unnecessary straying of components, which in-turn would cause GALFIT to crash or produce incorrect results.

3.4.1 J0437+2456

For this observation, the signal to noise ratio was too low to enable detailed analysis to be performed, which was probably due to bad weather. The **ellipse** task in IRAF was unable to follow the isophotes very far from the center. The GALFIT model does match the data and can be seen in the residual image in figure 7. The Sérsic component was found first and the initial values were changed slightly each time to see if the results differed. A PSF component was added after the residual for the Sérsic component showed a bright center.

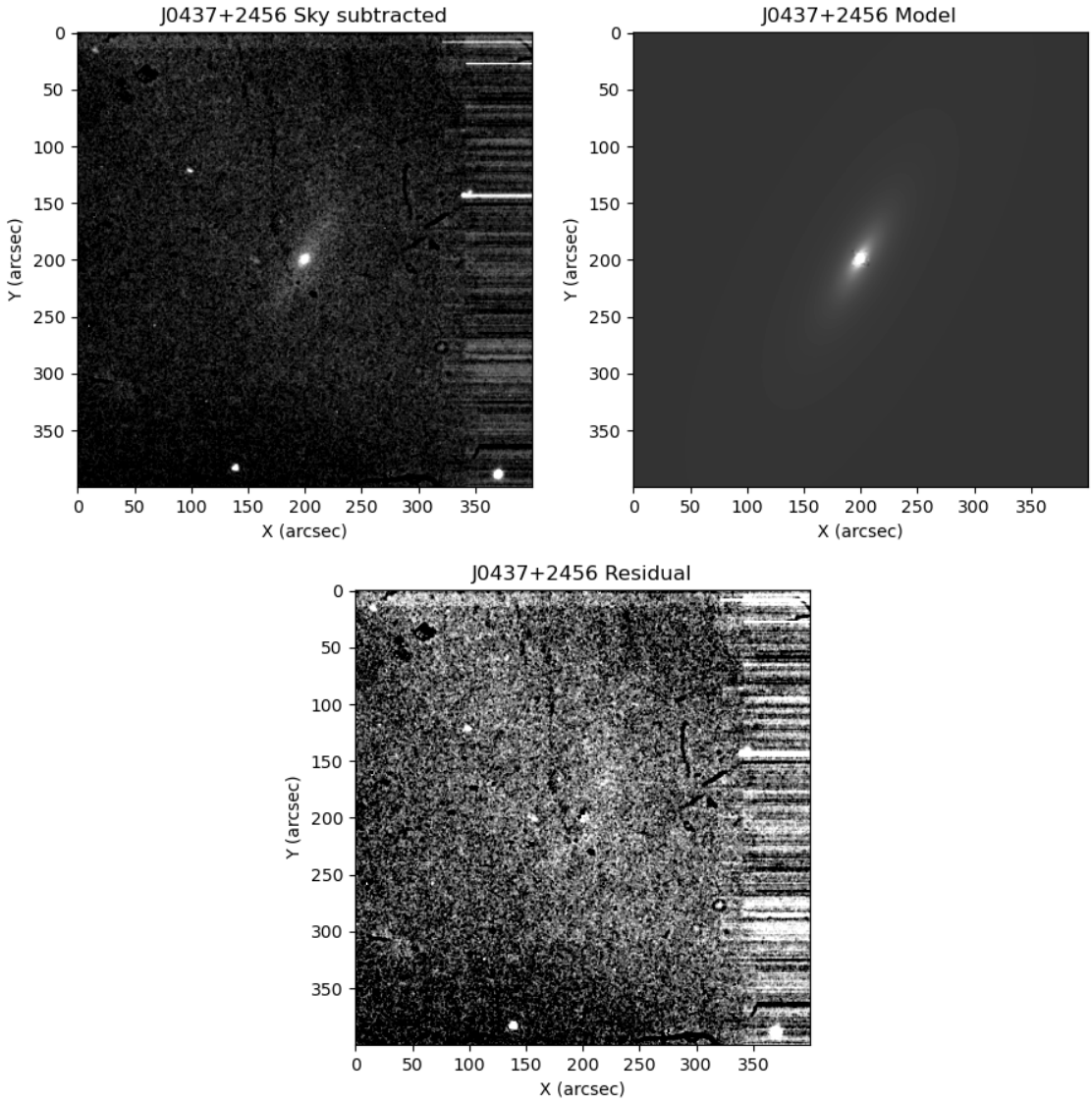

Figure 7. Top left image shows the combined sky subtracted image. Top right shows the GALFIT model and the bottom image shows the residuals from the GALFIT fitting.

3.4.2 NGC 5879

A Sérsic component was first used on the galaxy, where the starting parameters were chosen to be close to the magnitude values of the galaxy found in the 2MASS catalog. The results from the first fitting were then used as new starting parameters to run GALFIT again. The same procedure was used for multiple passes to achieve the best fit results. Each component was often fit separately, before fitting multiple components for a final result. The model was fitted with a Sérsic and disc. The residual image in figure 8 shows some remaining structures that could be spiral arms.

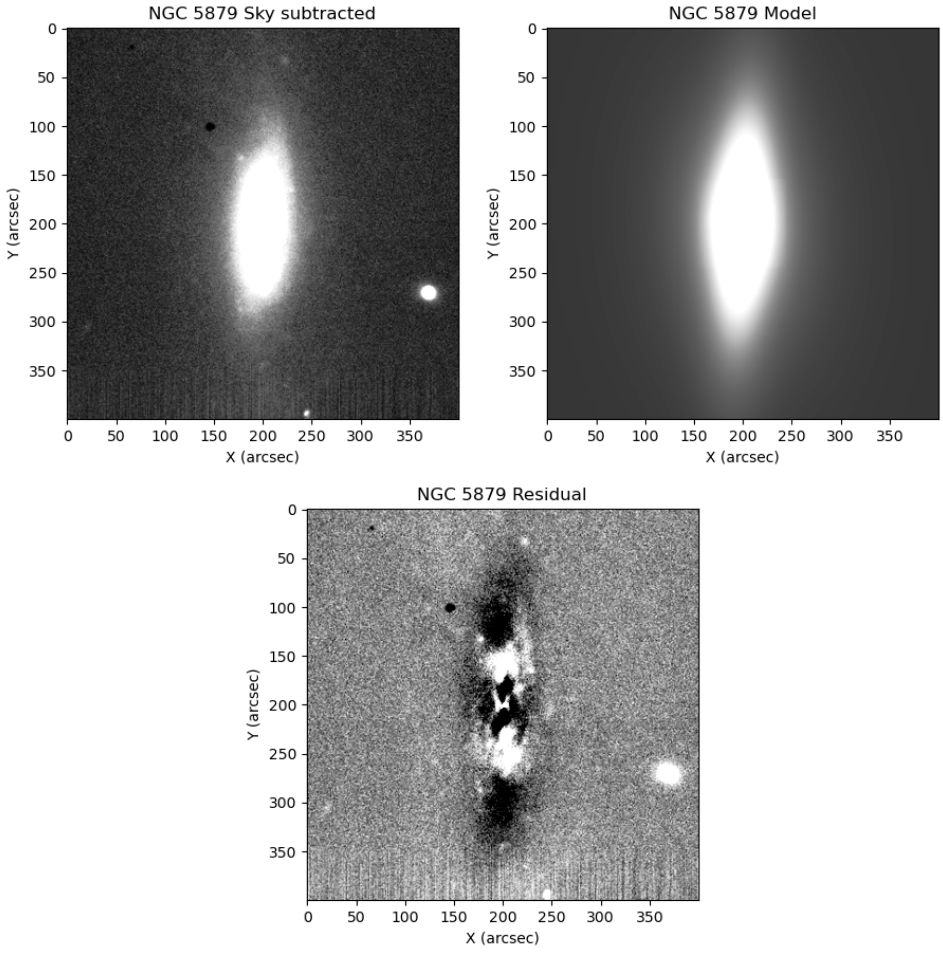

Figure 8. Top left image shows the combined sky subtracted image. Top right shows the GALFIT model and the bottom image shows the residuals from the GALFIT fitting.

3.4.3 NGC 6086

The residual in figure 9 shows some remaining structure of the galaxy. The model was fitted with a Sérsic and disc. The Sérsic component was found without fixing any parameters. The disk component was found using a similar procedure for the first galaxy. The two components were then used together to produce the final magnitudes.

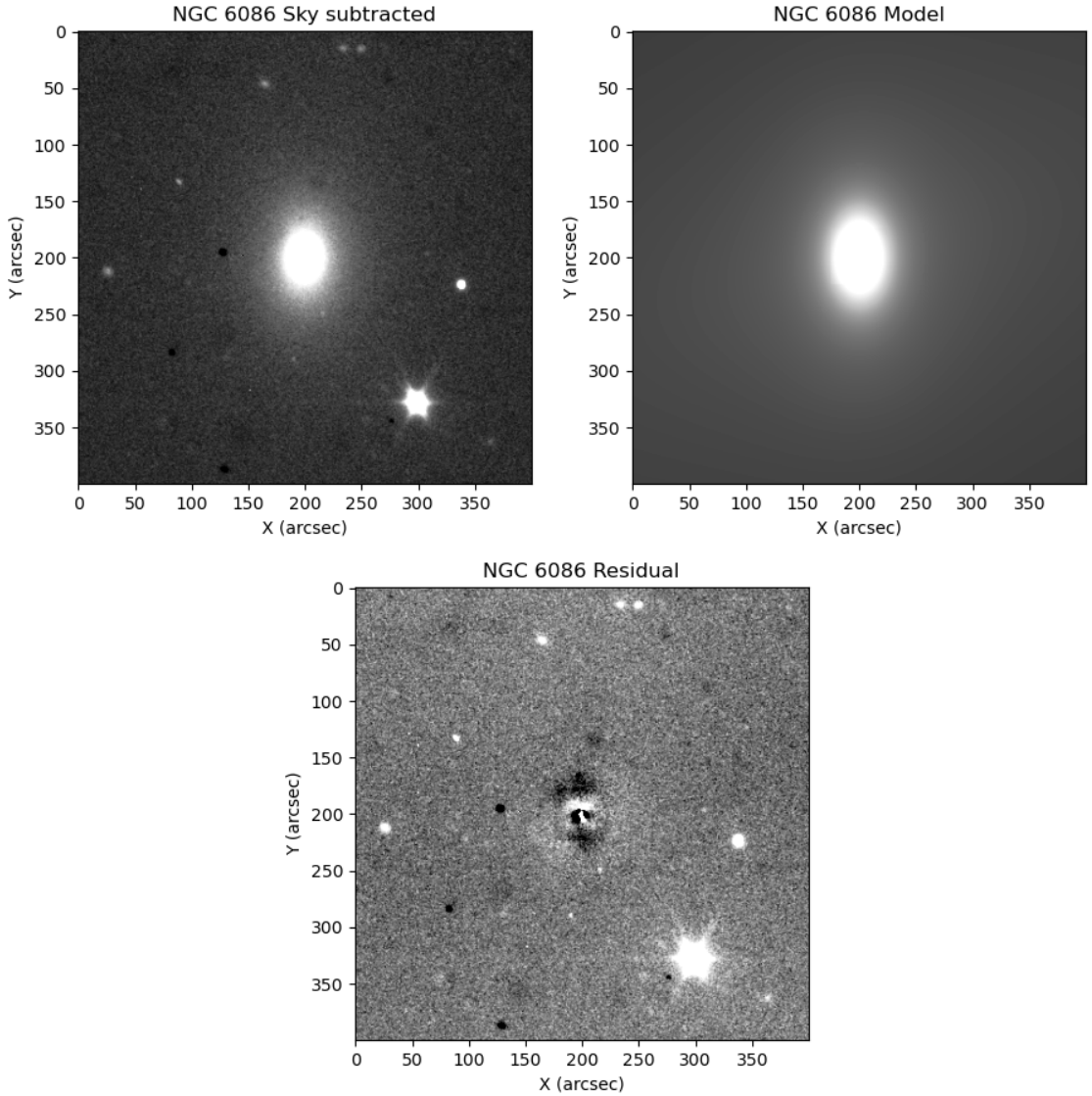

Figure 9. Top left image shows the combined sky subtracted image. Top right shows the GALFIT model and the bottom image shows the residuals from the GALFIT fitting.

3.4.4 NGC 6500

The residual in figure 10 shows remaining structure in the disc of the galaxy. The model was fitted with a Sérsic and disc. A Sérsic component was used first with a fixed Sérsic value of 4.0. The Sérsic index was then let loose as having it at 4.0 crashed the program often. The parameters of the individual components and the joint components were found after several passes of GALFIT.

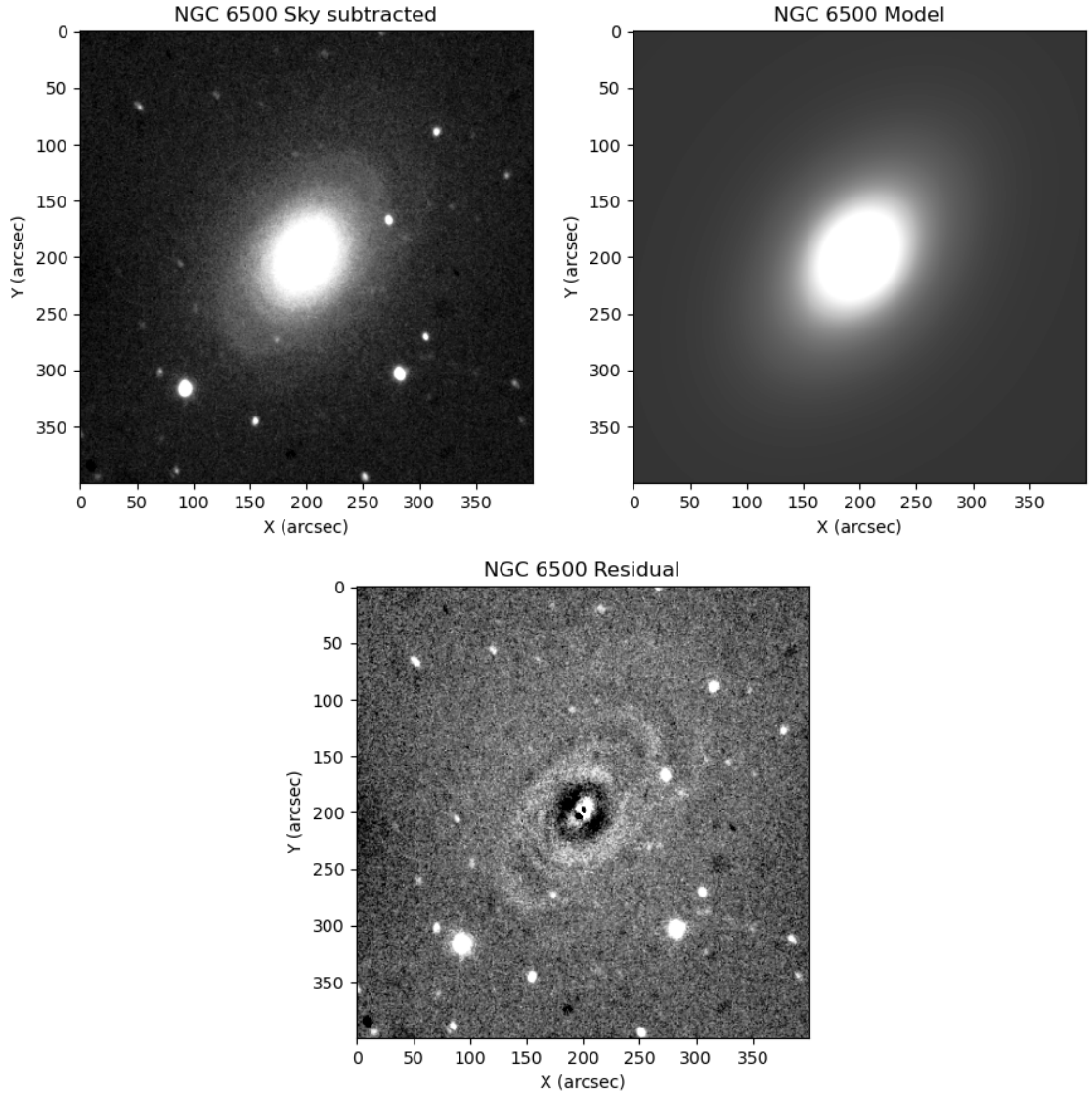

Figure 10. Top left image shows the combined sky subtracted image. Top right shows the GALFIT model and the bottom image shows the residuals from the GALFIT fitting.

3.4.5 UGC 12064

The residual in figure 11 shows very little remaining structure of the galaxy. The model was fitted with a Sérsic and bulge. A Sérsic component was used first with a fixed Sérsic value of 4.0. The disk component was then found before using both components at the same time.

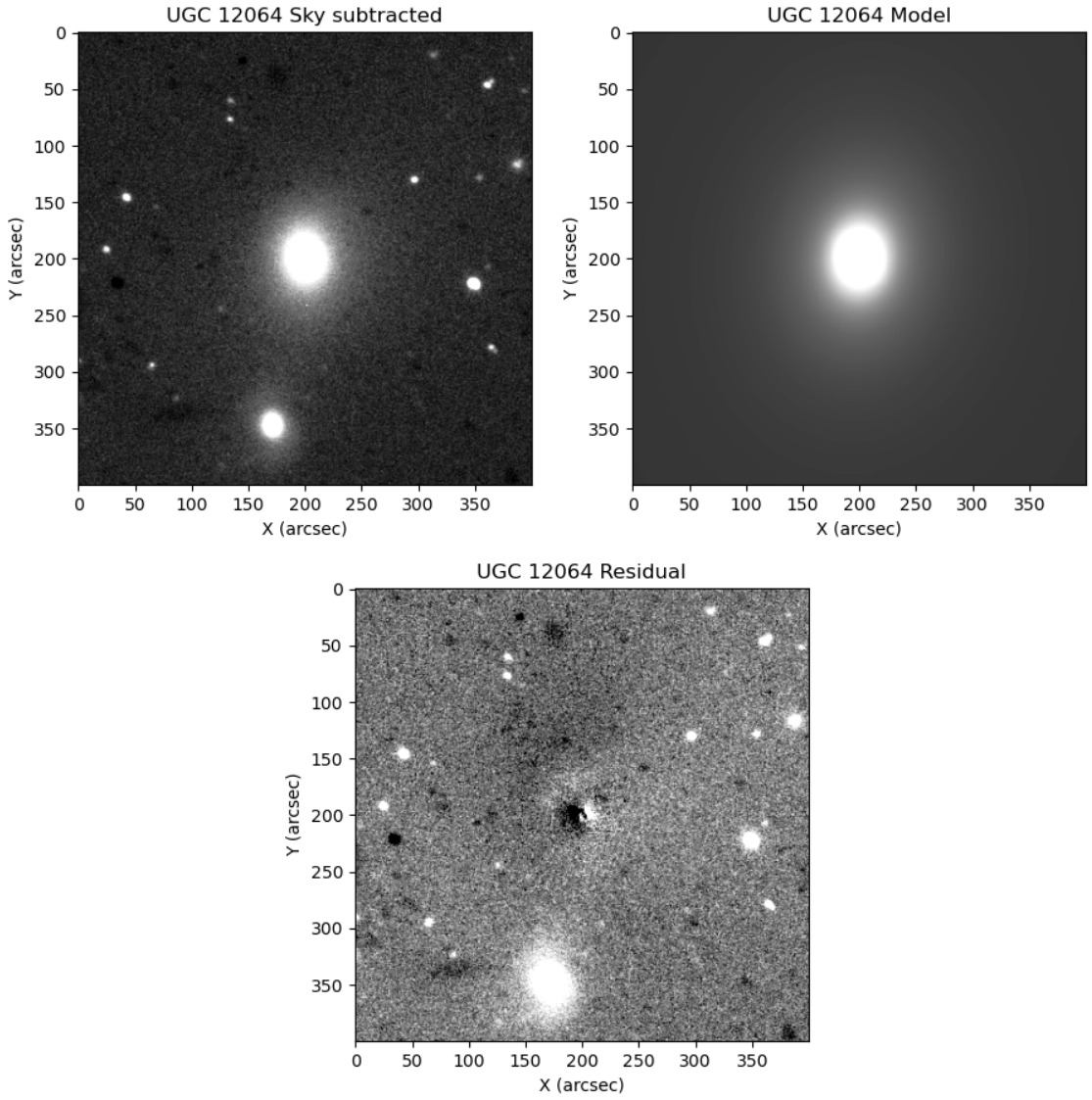

Figure 11. Top left image shows the combined sky subtracted image. Top right shows the GALFIT model and the bottom image shows the residuals from the GALFIT fitting.

3.4.6 NGC 7332

The residual in figure 12 shows complex structure of the galaxy, which may be from the bulge and disc. The galaxy being an edge on galaxy may have cause inaccurate values in galfit. The nucleus shows up in the residual and the difference in the apparent magnitudes are probably due not fitting the other components. A Sérsic component was used first with a fixed Sérsic value of 4.0. The disk component was then found. Both components were used where the Sérsic index was initial held fixed.

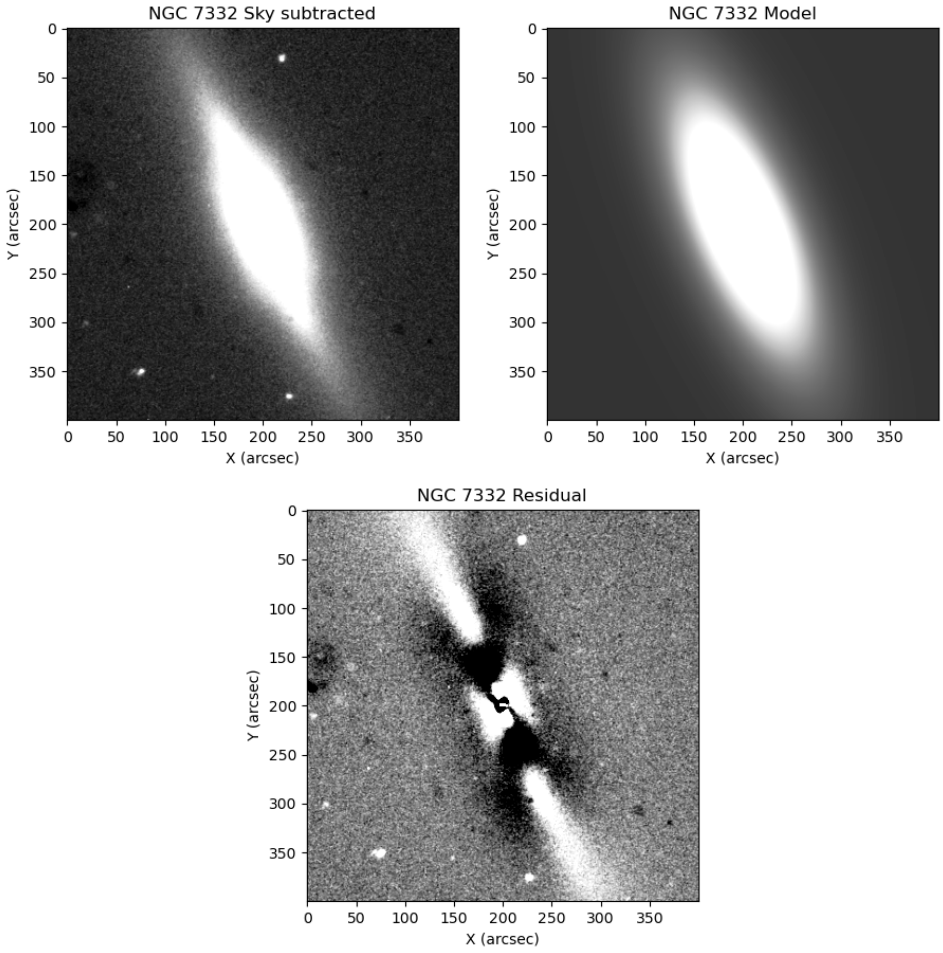

Figure 12. Top left image shows the combined sky subtracted image. Top right shows the GALFIT model and the bottom image shows the residuals from the GALFIT fitting.

3.4.7 NGC 7469

The residual in figure 13 shows a halo structure of the galaxy that was not fitted. The model was fitted with a Sérsic and disc. The Sérsic component was found without fixing any parameters several times with different initial values to see of the results were the same. The disk component was found, then the two components were they used together, firstly fixing the Sérsic index to 4.0. The ring structure and possiblly more internal structures were difficult for GALFIT to run. A PSF component was added as the center was very bright. The three components were run producing the final model and residuals seen.

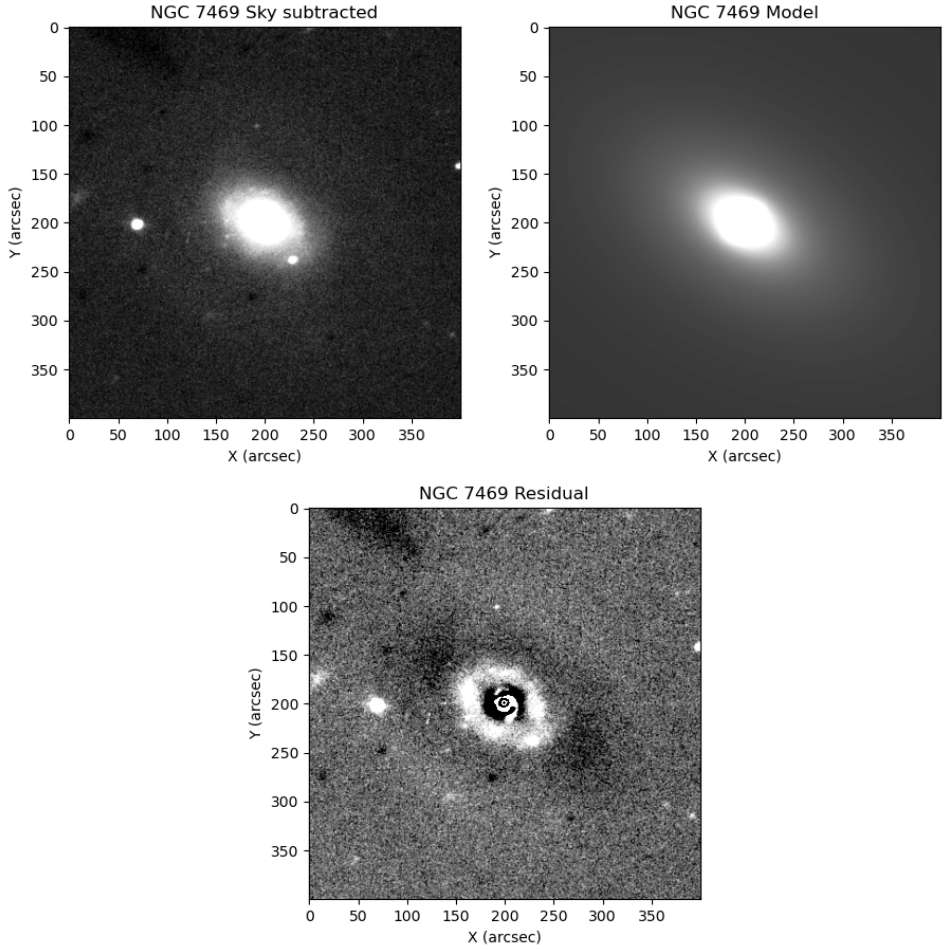

Figure 13. Top left image shows the combined sky subtracted image. Top right shows the GALFIT model and the bottom image shows the residuals from the GALFIT fitting.

3.4.8 IC 1481

The residual in figure 14 shows very little remaining structure of the galaxy. The model was fitted with a Sérsic and disc. A Sérsic component was used first with a fixed Sérsic value of 4.0. The disk component was then found, where the initial values differed slightly to see if the results were similar. Both components were used where the Sérsic index was initial held at first, then let loose, before finding reasonable parameters after many runs of GALFIT. The second galaxy is brighter and may have caused contamination with light even though it was masked out. A PSF component was added after as the center was very bright.

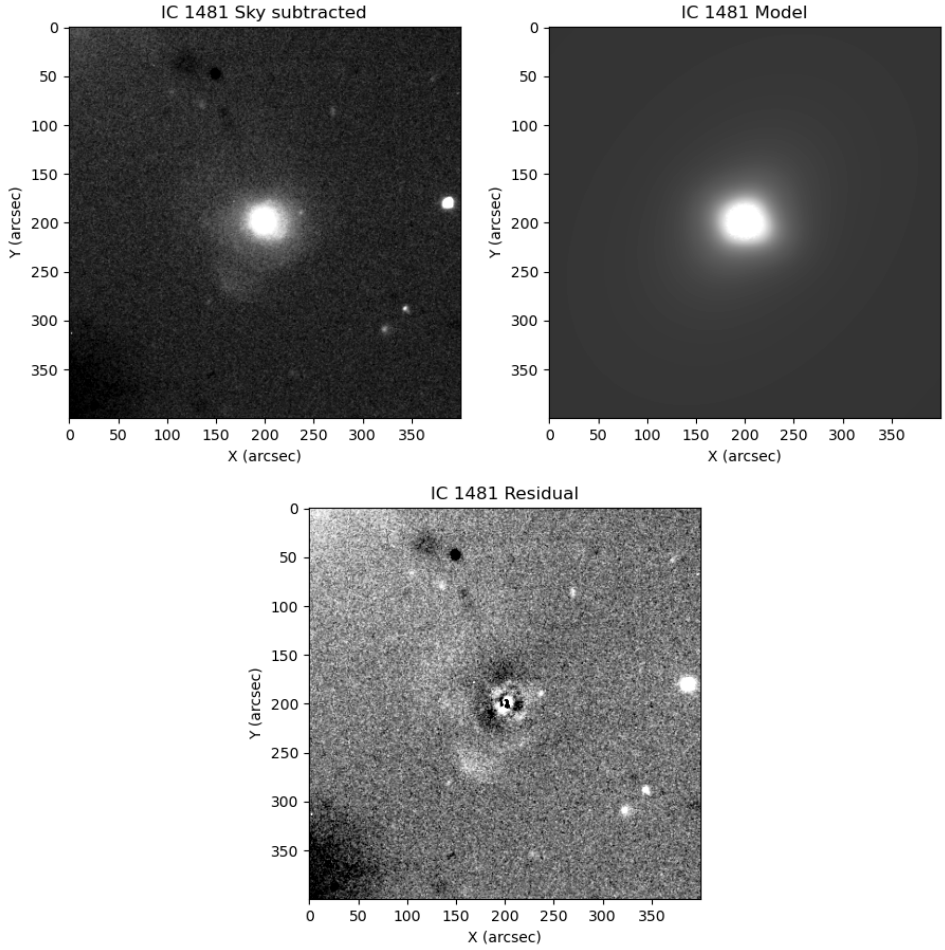

Figure 14. Top left image shows the combined sky subtracted image. Top right shows the GALFIT model and the bottom image shows the residuals from the GALFIT fitting.

3.4.9 NGC 7682

The residual in figure 15 shows possibly a nucleus as the remaining structure of the galaxy. The model was fitted with a Sérsic and disc. A Sérsic component was used first with a fixed Sérsic value of 4.0. The disk component was then found, then both components were used. The initial Sérsic produced error was fixed at a Sérsic index of 4.0 until the other parameters converged. The error that occurred could be from a potential bar in the galaxy which could not be fitted.

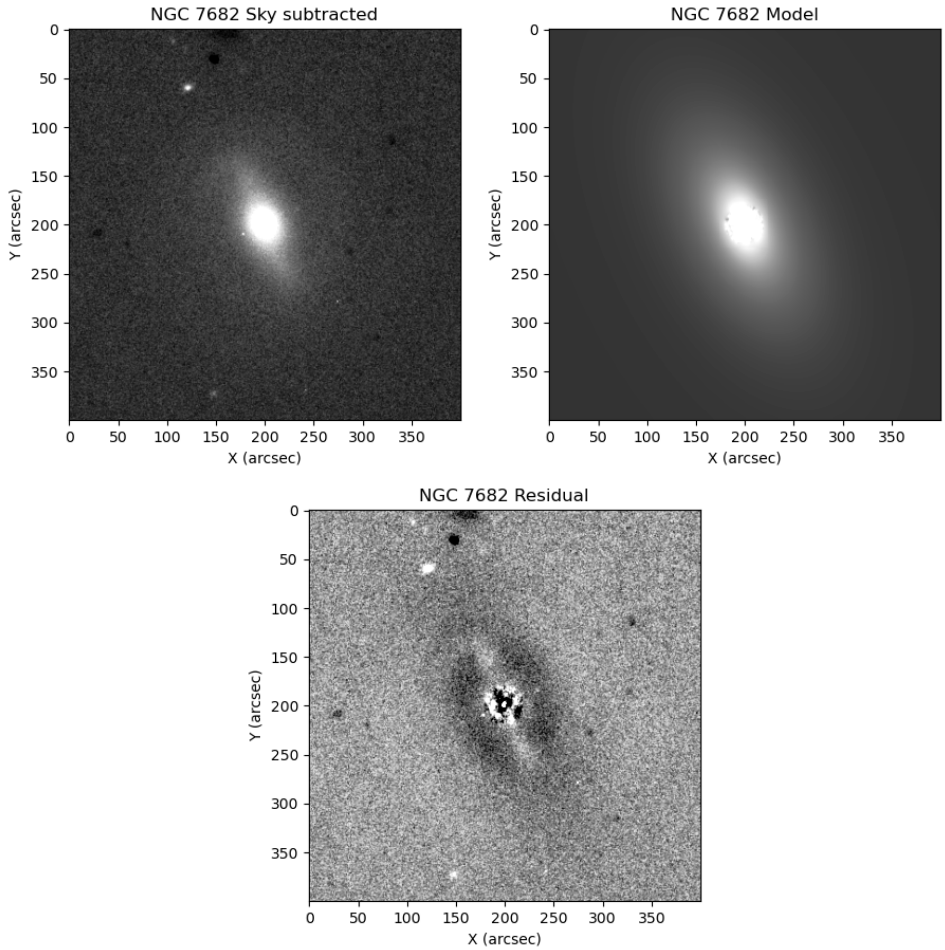

Figure 15. Top left image shows the combined sky subtracted image. Top right shows the GALFIT model and the bottom image shows the residuals from the GALFIT fitting.

3.5 Post GALFIT analysis

Once GALFIT reached its results, the **ellipse** task in IRAF was then used to find the values needed for making the surface brightness plots. The ellipse tables were made by fixing the center for each galaxy. The initial ellipticity and initial position angle given in the GALFIT final output file were used. The sma step of 0.1, the center ,the ellipticity and the position angle were not fixed. Integration mode was median and 2.5 sigma clipping at 1 iteration. **Tdump** task was used to get readable values in order to make the plots. An example of the tdump file is seen in figure 16.

Open

5879data.txt
/home/chants/Documents/2025/01-NGC5879

1	0.5730851	27736.17	164.4065
2	0.6303936	27662.28	178.9491
3	0.693433	27581.52	194.7877
4	0.7627763	27493.93	211.9546
5	0.839054	27403.13	229.8303
6	0.9229594	27304.96	249.3214
7	1.015255	27199.8	270.455
8	1.116781	27081.9	292.7412
9	1.228459	26866.74	320.8759
10	1.351305	26495.34	345.305
11	1.486435	26074.85	365.7253
12	1.635079	25659.05	383.5751
13	1.798587	25186.65	401.3473
14	1.978446	24626.18	425.7996
15	2.17629	23931.18	456.8452
16	2.393919	23162.89	445.8092
17	2.633312	22318.87	422.4073
18	2.896643	21332.49	402.7639
19	3.186307	20325.58	367.6218
20	3.504938	19376.85	320.2043
21	3.855432	18402.85	286.079
22	4.240975	17450.32	257.1963
23	4.665072	16562.12	227.8269
24	5.13158	15642.71	207.3567
25	5.644738	14679.71	178.223
26	6.209212	13765.4	156.0505
27	6.830134	12931.09	133.3071
28	7.513147	12153.65	116.1712
29	8.264462	11392.31	102.0154
30	9.090909	10619.	90.20464
31	10.	9900.599	81.53922
32	11.	9213.01	73.98959

Figure 16. Example tdump file containing Semi major axis, intensity and intensity error.

4 Results and Discussion

4.1 General results

The GALFIT results for Sérsic and disk decomposition can be seen in table 2. Only the Sérsic and disk components were used. The absolute magnitudes were calculated using the distance modulus formula, equation (5).

$$m - M = 5lg(r) - 5 \tag{5}$$

Where r is, the distance in megaparsecs.

Results of GALFIT modeling

(1) Object	(2) Black hole Mass ($M_\odot$)	(3) PSF Magnitude	(4) M_b	(5) R_e	(6) n	(7) M_d	(8) R_s	(9) χ^2	(10) M_{Total}
J0437+2456	6.45±0.03	14.9	11.6	77.6	4.1	0.0	0.0	1.3	-22.5
NGC 5879	$6.62^{+0.28}_{-6.62}$		9.4	78.0	4	9.7	44.2	1.4	-20.7
NGC 6086	9.57±0.17		10.0	33.8	4	8.5	387.1	0.8	-25.7
NGC 6500	8.34±0.26		10.4	9.5	2.6	10.0	33.8	0.8	-22.4
UGC 12064	8.84±0.52		9.6	71.1	4	11.7	5.3	0.4	-23.1
NGC 7332	7.08±0.18		8.7	6.2	4	7.6	48.9	3.0	-22.9
NGC 7469	6.94±0.16	10.4	9.4	112.7	4	10.4	4.6	18.8	-24.0
IC 1481	7.15±0.13	12.7	10.6	81.3	4	11.8	14.7	1.5	-24.1
NGC 7682	7.56±0.33		11.2	13.6	4	10.1	53.1	1.1	-22.7

Table 2. Table shows the results for galfit-Column 2 shows the Black hole mass. Colume 3 shows the PSF magnitude. Column 4,5 and 6 show the Sérsic component with magnitude, effective radius and the Sérsic value. Columns 7 and 8 show the disc component with magnitude and effective radius. Column 9 shows theχ^2value and column 10 absolute bulge magnitude.

4.2 J0437+2456

J0437+2456 is a spiral galaxy at a distance of 66.0 Mpc away. The signal to noise ratio being too low made it difficult to enable detailed analysis to be performed, which was probably due to bad weather The bulge magnitude was found to be 11.6 the PSF magnitude of 14.9. The apparent K-band magnitude found on the 2MASS catalog was 12.6. The absolute bulge magnitude was calculated to be -22.5.

4.3 NGC 5879

NGC 5879 is an SA galaxy at a distance 10.6 Mpc. The bulge apparent magnitude was found to be 9.4 and the K-band magnitude is 11.2. The absolute magnitude of the bulge was calculated to be -20.7. The plot shows a steep bulge at 5 arcsec. The model closely fits the data and it shows a slight increase at around 7 arcsec which would be caused by spiral arms in the galaxy.

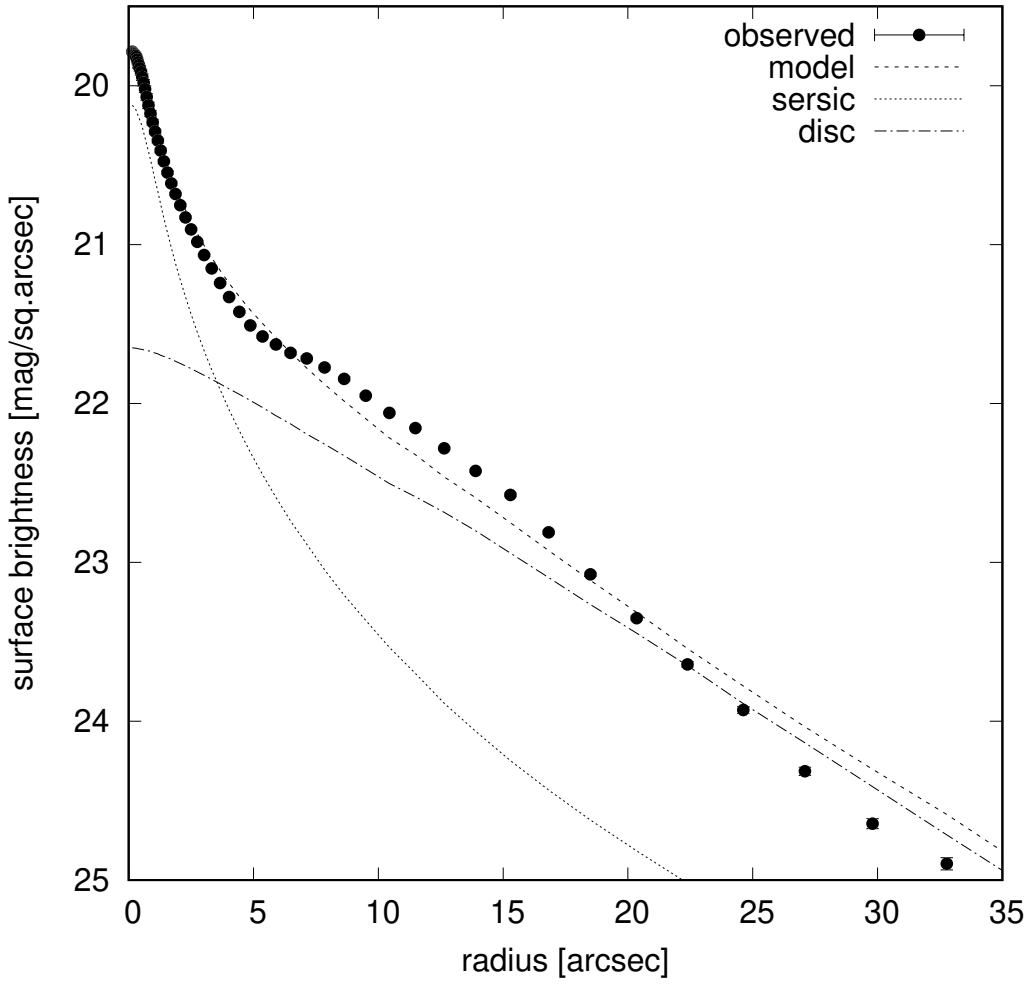

Figure 17. Decomposition of NGC 5879.The plot show the surface-brightness profile in mag/arcsec^2 and the SMA in arcsec.The plot shows the data, the model, Sérsic and exponential components generated by GALFIT.

4.4 NGC 6086

NGC 6086 is an E galaxy at a distance 138.0 Mpc. The plot of the data and the model are very close.The bulge apparent magnitude is higher than the 2MASS magnitude, where the data showed it to be 10 and the 2MASS K-band magnitude, 11.58. The absolute magnitude of the bulge was calculated to be -25.7. The model fits and the Sérsic fit the data very closely and the disc was found to be very low in magnitude compared to the Sérsic.

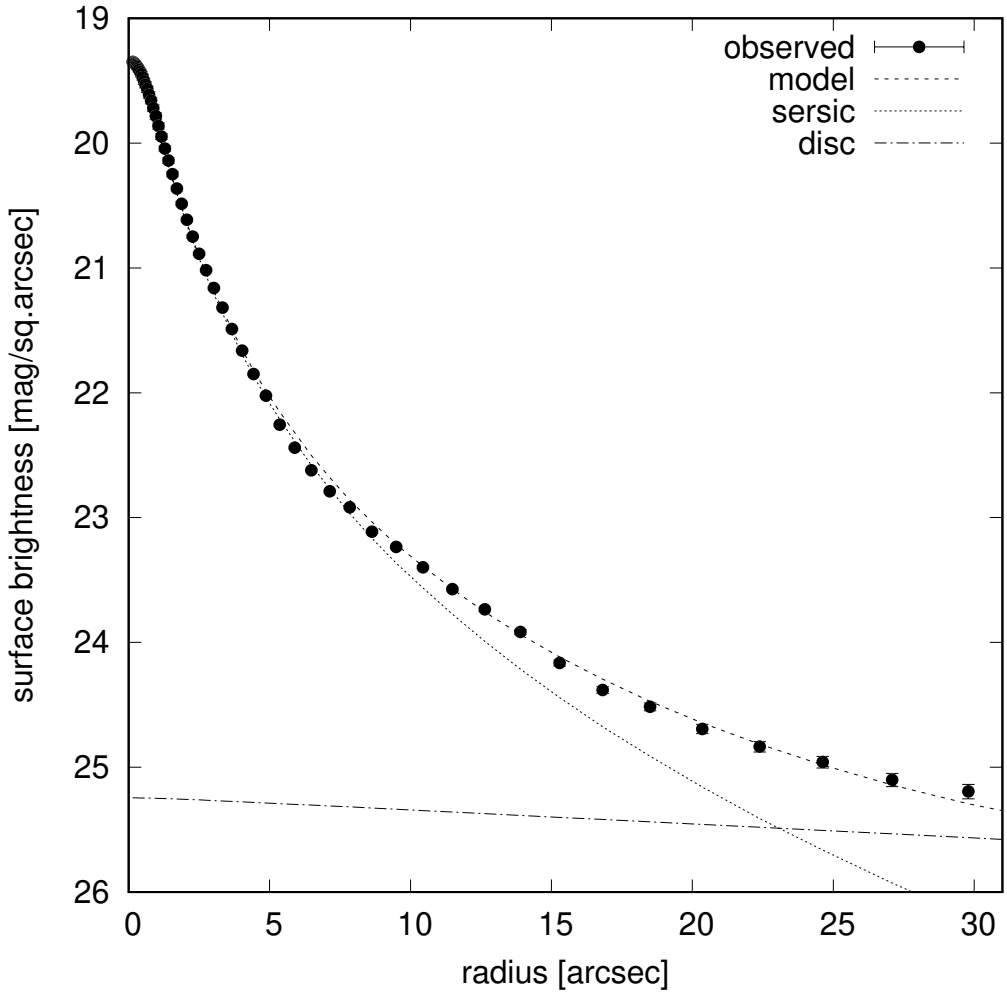

Figure 18. Decomposition of NGC 6086,The plot show the surface-brightness profile in mag/arcsec^2 and the SMA in arcsec.The plot shows the data, the model, Sérsic and exponential components generated by GALFIT.

4.5 NGC 6500

NGC 6500 is an SA galaxy at a distance 36.5 Mpc. The bulge apparent magnitude is 10.6 and the K-band magnitude is 10.6. The absolute magnitude of the bulge was calculated to be -22.4. The Sérsic is steep in the plot and the disc is bright in this galaxy.

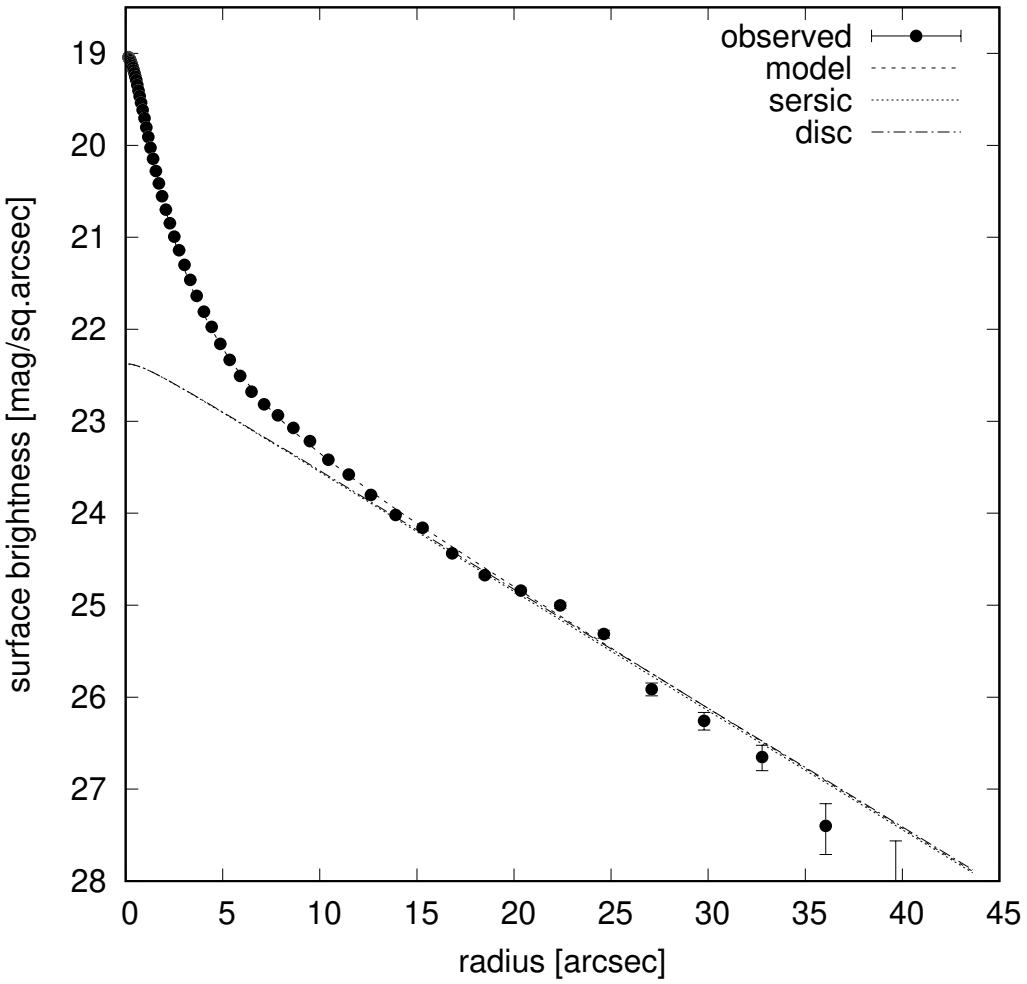

Figure 19. Decomposition of NGC 6500,The plot show the surface-brightness profile in mag/arcsec^2 and the SMA in arcsec.The plot shows the data, the model, Sérsic and exponential components generated by GALFIT.

4.6 UGC 12064

UGC 12064 is an S0 galaxy at a distance 34.7 Mpc. The bulge apparent magnitude was found to be 9.6 and the K-band magnitude is 11.066. The absolute magnitude of the bulge was calculated to be -23.1. Both Sérsic and disc were bright in the galaxy.

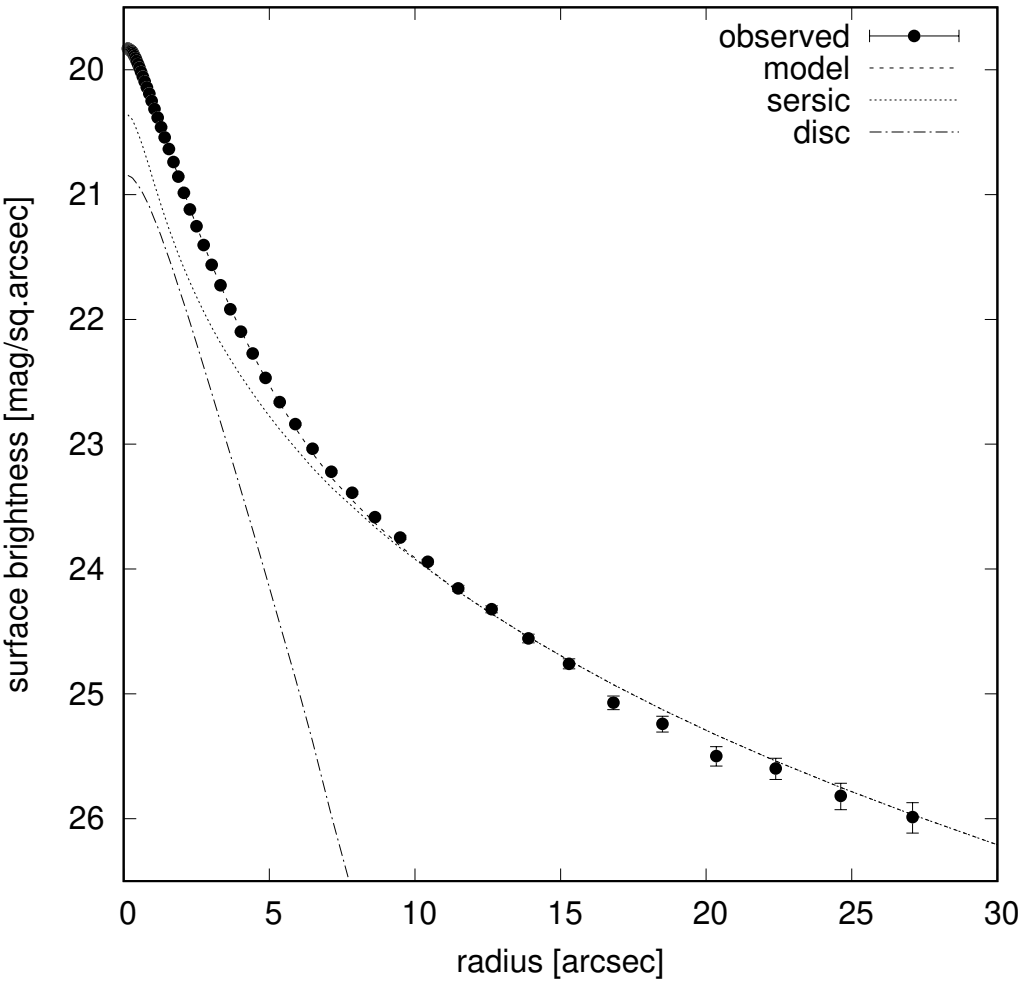

Figure 20. Decomposition of UGC 12064, The plot show the surface-brightness profile in mag/arcsec^2 and the SMA in arcsec.The plot shows the data, the model, Sérsic and exponential components generated by GALFIT.

4.7 NGC 7332

NGC 7332 is an S0 galaxy at a distance 21.7 Mpc. The bulge apparent magnitude is 8.7 and the K-band magnitude is 10.015. The absolute magnitude of the bulge was calculated to be -22.9. The Sérsic is steep within 10 arcsec and the disc is brighter after that.

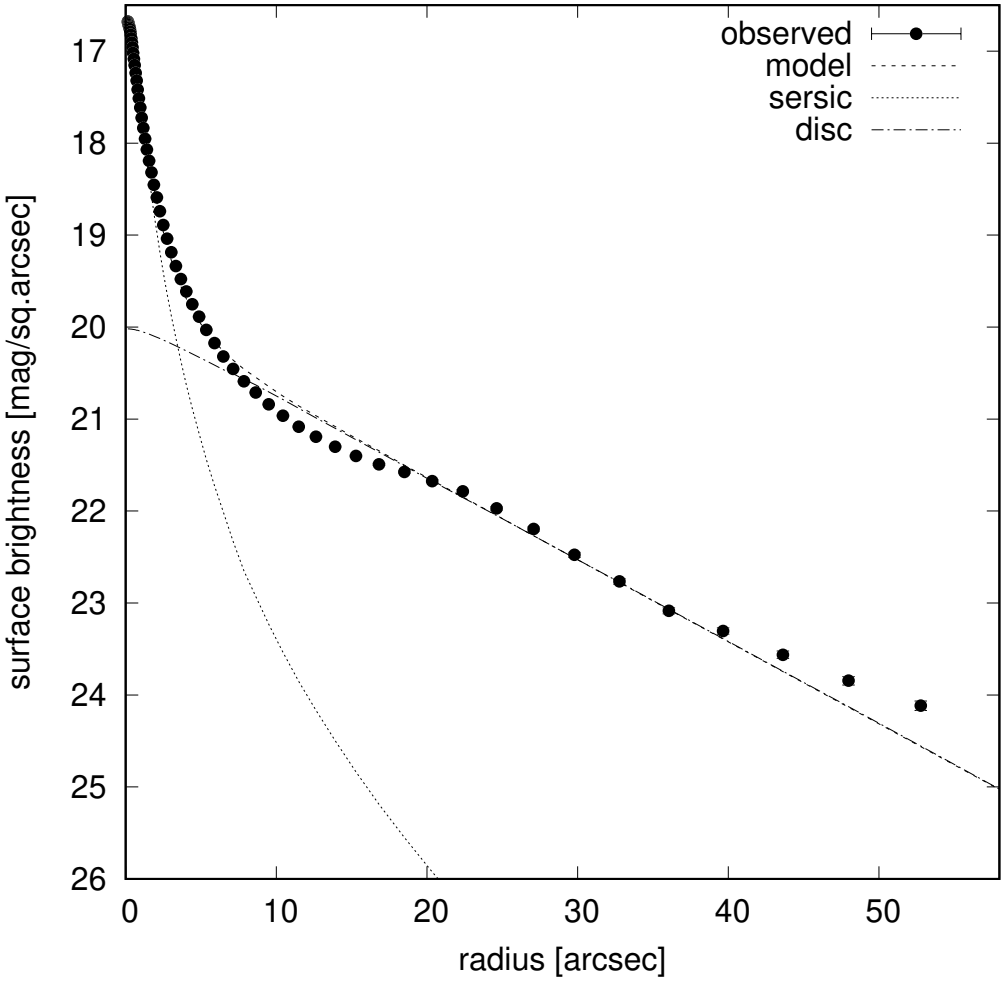

Figure 21. Decomposition of NGC 7332,The plot show the surface-brightness profile in mag/arcsec^2 and the SMA in arcsec.The plot shows the data, the model, Sérsic and exponential components generated by GALFIT.

4.8 NGC 7469

NGC 7469 is a spiral galaxy at a distance 47.7 Mpc. The bulge apparent magnitude is 9.4 and the K-band magnitude is 9.762. The PSF apparent magnitude was 10.4. The absolute magnitude of the bulge was calculated to be -24.0. The center is bright but smaller than the Sérsic. The disc becomes brighter than both. The model diverges from the data as the galaxy was complex leaving a residual ring around the core.

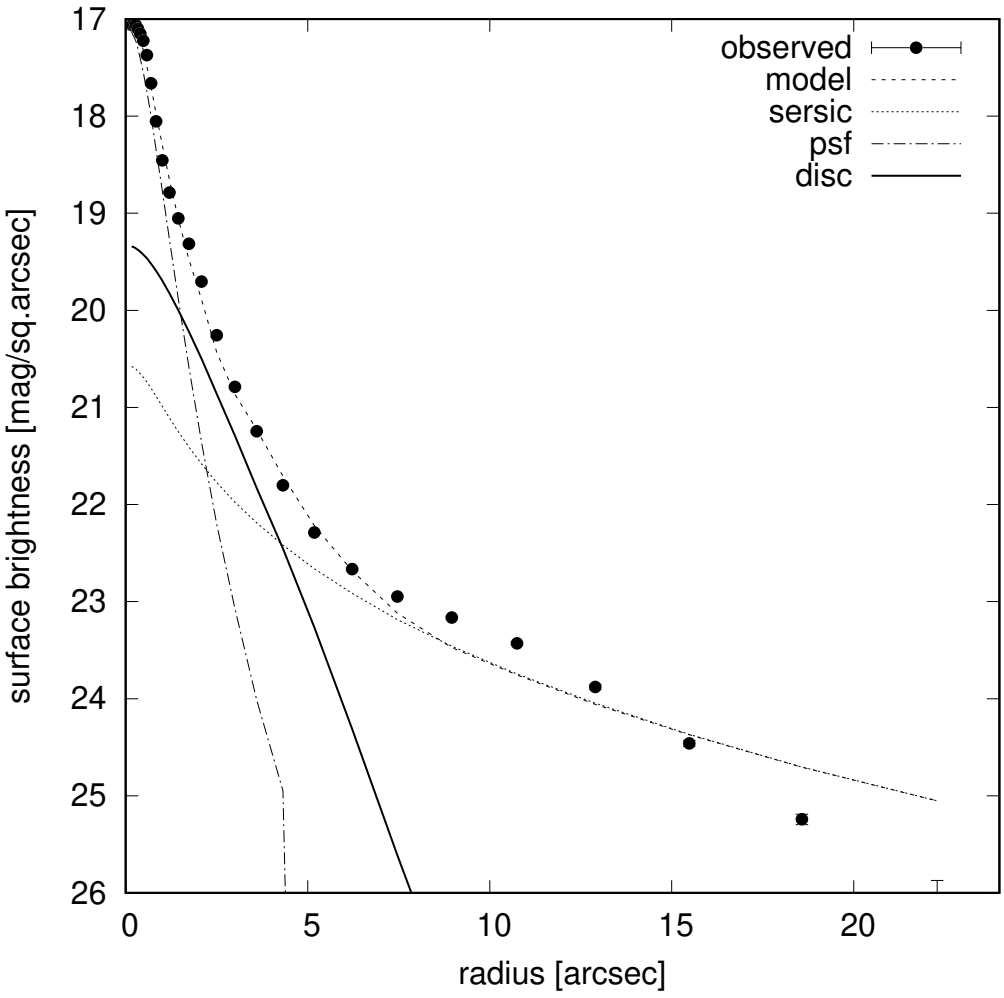

Figure 22. Decomposition of NGC 7469, The plot show the surface-brightness profile in mag/arcsec^2 and the SMA in arcsec.The plot shows the data, the model, Sérsic and exponential components generated by GALFIT.

4.9 IC 1481

IC 1481 is a spiral galaxy at a distance of 89.9 Mpc. The bulge apparent magnitude was found to be 10.6 and the K-band magnitude is 12.169. The absolute magnitude of the bulge was calculated to be -24.1. The center is bright and a PSF was needed to model the galaxy. The disc and Sérsic were both present in the galaxy.

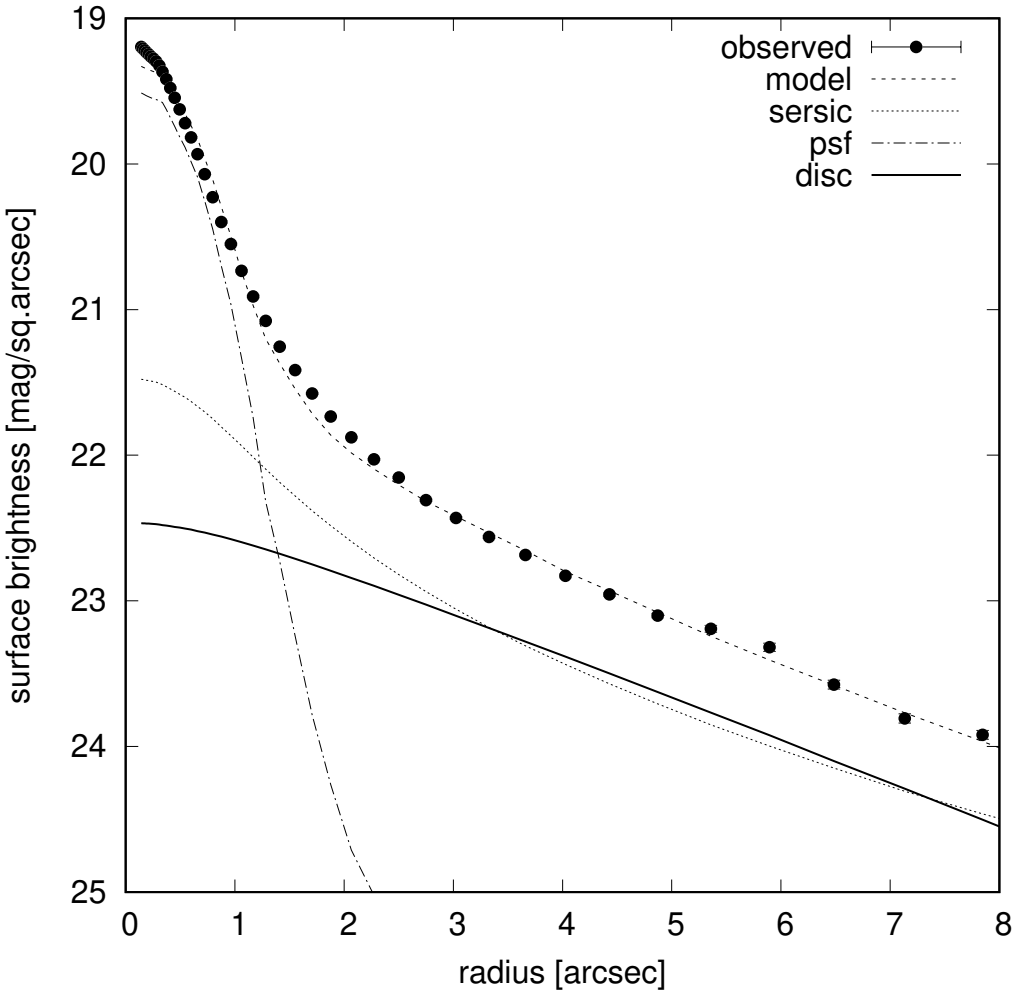

Figure 23. Decomposition of IC 1481,The plot show the surface-brightness profile in mag/arcsec^2 and the SMA in arcsec.The plot shows the data, the model, Sérsic and exponential components generated by GALFIT.

4.10 NGC 7682

NGC 7682 is an SB galaxy at a distance 59.3 Mpc. The bulge apparent magnitude was found to be 11.2 and the K-band magnitude is 12.2. The absolute magnitude was calculated to be -22.7. The bulge is bright until around 5 arcsec where the disc is more prominent.

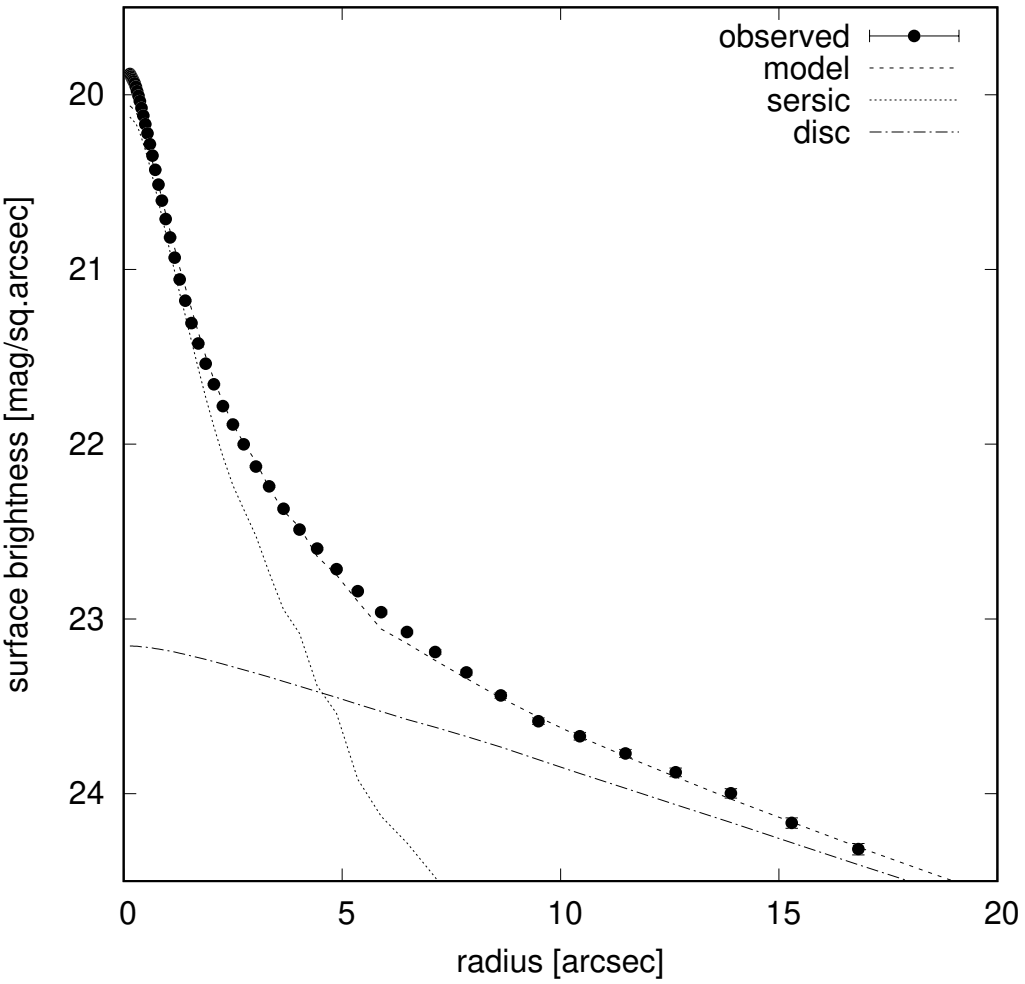

Figure 24. Decomposition of NGC 7682, The plot show the surface-brightness profile in mag/arcsec^2 and the SMA in arcsec.The plot shows the data, the model, Sérsic and exponential components generated by GALFIT.

4.11 Discussion

How coevolution works within the galaxy is still an unanswered question in astronomy. The feedback of the black hole regulating the growth of the host galaxy or the stellar environments that regulate the growth of the black hole are two ways in which the black holes co evolves with their host galaxy. To understand this mechanism more, we need to further explore black hole-host galaxy relations [21]. There has been many ongoing research that shows there may be correlations between the host galaxy and supermassive black hole mass and it has been shown that there may be co-evolution with the black hole and the host galaxy [21]. In the paper [22] they have suggested that the black hole mass may be correlated with the bulge luminosity and not with the total host galaxy luminosity. While [11] have found several relations between the black hole and the host galaxy.

With early type galaxies [23]found that the bulge luminosity and total host galaxy luminosity correlate better with the black hole mass. In this study the bulge absolute magnitude was found for several host galaxies and was compared to the black hole mass. This was done to help understand the relation between them and to further understand galaxy evolution.

It has been found that active galaxies do not follow a BH mass-Bulge luminosity relation [21] by several authors. One author [24] showed that there was deviation of one magnitude in the brightness of the bulge possibly due to young stellar populations, whereas [25]argue that their deviation may have been from growing black holes. In a study [26]shows that active galaxies with low-mass black holes fell below the linear Black hole mass-bulge luminosity relation of inactive galaxies, which also had a 1 magnitude offset in the bulge luminosity. Some galaxies in this study were active galaxies and that may be the reason for the current correlation in the figure 25.

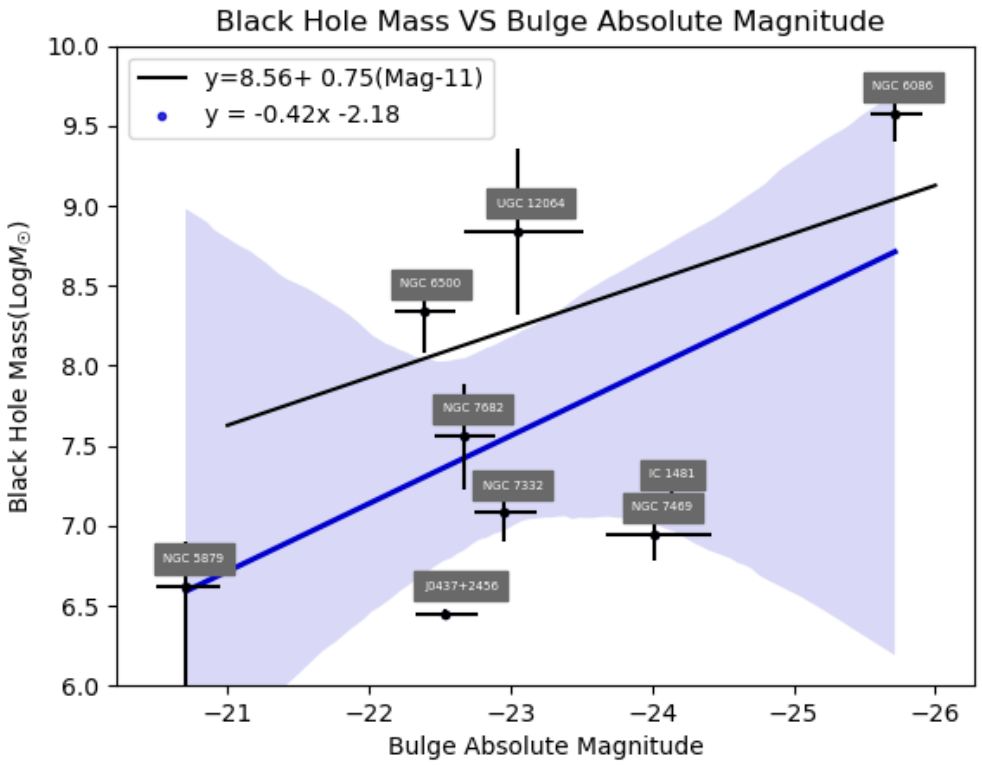

Figure 25. Black hole Mass against Bulge Absolute magnitude. The confidence level is 95% shown by the pale blue band. The solid blue line represents the best fit line for the give data set with the form y= -042.x -2.18. The black line is the best fit relation from [23] where the line was converted from (L_b, std) to M, taking the form y=8.56+ 0.75(Mag-11).

Based on the data presented here, the figure 25 shows the correlation with the black hole mass and the bulge absolute magnitudes. The few galaxies that are far from the line may have had bad fitting due to other complex structures in the galaxy or bright nuclei. The line shows that the magnitudes increase with larger black hole masses. In the figure 26 their data also show an increase of magnitude with increasing BHmass within a similar range.

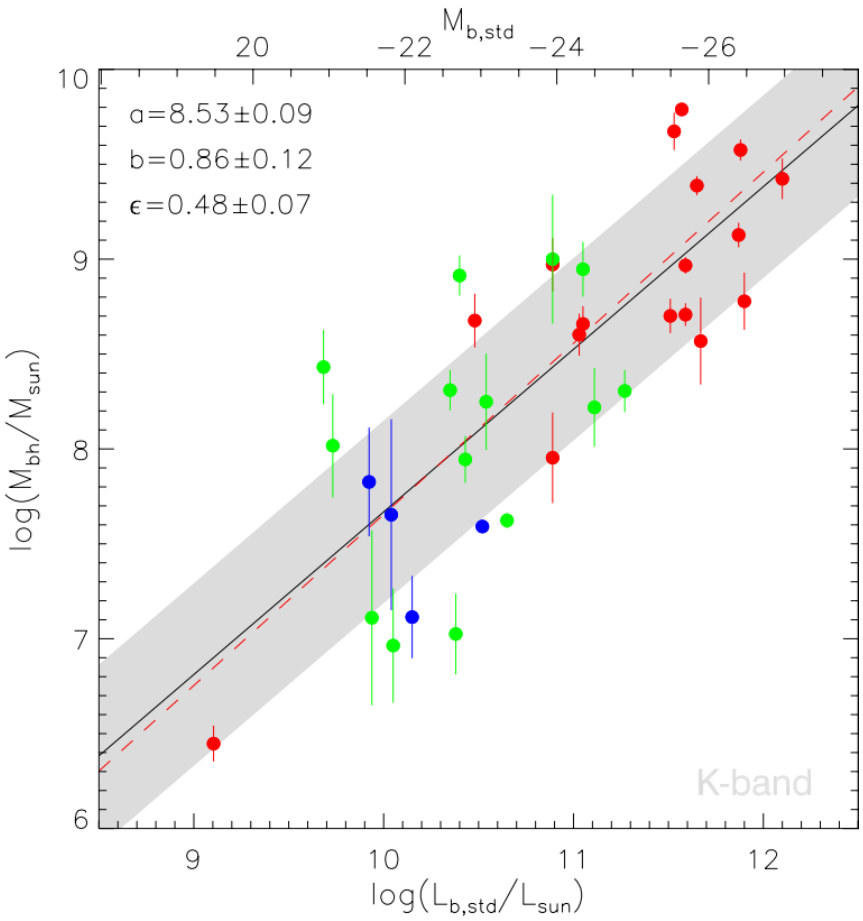

Figure 26. Here [23] shows the correlation between $M_\bullet$ and standard bulge (L_b, *std*) in their data. The red circles correspond to elliptical, the green S0, and the blue are spiral galaxies. Vertical solid bars indicate a 1σ-uncertainties in $M_\bullet$. The solid black lines correspond to the best-fit linear relations of the form log $M_\bullet$ = a + b(logL - 11). The shaded area has a width of $2\epsilon_\bullet$ in the direction of $M_\bullet$.

In their research [27] found that with GALFIT , some models with high Sérsic values had more uncertainties and caused systematic errors which was resolved by fixing the Sérsic to n=6. During the analysis of GALFIT the Sérsic was set to n=4 for most galaxies, as the the program had trouble converging to a reasonable value. It was found that in[28], errors could be explained with the complexity in the objects,either having bars, spiral arms, or bending discs. This could be the problem with some galaxies in this study, as some of the targets were quite complex. Despite the complexity of the galaxies the correlation seemed to be similar to other papers.

5 Conclusion

2-D structural decomposition was performed on 9 galaxies in the K-band magnitude. The galaxies in the data set were found to have similar apparent magnitudes to that which was previously found using other methods, within the 2MASS catalog. Out of the original data set, 3 had bad data, which could not be used. J0437+2456 was very faint in the images making it difficult to get accurate results, possibly due to bad weather at the time. Most the galaxies were fitted when the final χ^2 value was reduced to one. Most galaxies were Spiral with one elliptical which could be fitted with a Sérsic component only. The results would be more accurate if other components such as bars and arms were also fitted, which was beyond the scope of the thesis. The plots of the models were close to the data, making it easy to determine if there were other complex structures. The accuracy in the magnitudes could be improved by adding components to the decomposition's and using different PSF models. Figure 25 and figure 26 shows that the increase of magnitude with size. The galaxies were early type galaxies ranging from BH masses of $10^6 M_\odot$ to $10^9 M_\odot$ to show that they may correlate better with the total bulge luminosity. While this thesis showed a small part of a correlation with BHmass and bulge magnitude there are other correlations that can help in the studying of the potential coevolution of the BHmasses and their host galaxies in future work.

6 Appendix

```
# IMAGE PARAMETERS
A) gal.fits            # Input data image (FITS file)
B) imgblock.fits       # Output data image block
C) none                # Sigma image name (made from data if blank or "none")
D) psf.fits   #        # Input PSF image and (optional) diffusion kernel
E) 1                   # PSF fine sampling factor relative to data
F) none                # Bad pixel mask (FITS image or ASCII coord list)
G) none                # File with parameter constraints (ASCII file)
H) 1    93   1    93   # Image region to fit (xmin xmax ymin ymax)
I) 100    100          # Size of the convolution box (x y)
J) 26.563              # Magnitude photometric zeropoint
K) 0.038  0.038        # Plate scale (dx dy)   [arcsec per pixel]
O) both                # Display type (regular, curses, both)
P) 0                   # Options: 0=normal run; 1,2=make model/imgblock & quit

# INITIAL FITTING PARAMETERS
#
#   For object type, the allowed functions are:
#       nuker, sersic, expdisk, devauc, king, psf, gaussian, moffat,
#       ferrer, and sky.
#
#   Hidden parameters will only appear when they're specified:
#       C0 (diskyness/boxyness),
#       Fn (n=integer, Azimuthal Fourier Modes).
#       R0-R10 (PA rotation, for creating spiral structures).
#
# ------------------------------------------------------------------------------
#   par)    par value(s)    fit toggle(s)    # parameter description
# ------------------------------------------------------------------------------

# Object number: 1 -- A TRUE point source
 0) psf                    #    Object type
 1) 50.00  50.00  1 1      #  position x, y
 3) 18.000     1           #  total magnitude
 Z) 0                      #  Output option (0 = residual, 1 = Don't subtract)

# Object number: 2
 0) sersic                 #  object type
 1) 48.5180  51.2800  1 1  #  position x, y
 3) 20.0890     1          #  integrated magnitude
 4) 5.1160      1          #  R_e (half-light radius)   [pix]
 5) 4.2490      1          #  Sersic index n (de Vaucouleurs n=4)
 9) 0.7570      1          #  axis ratio (b/a)
10) -60.3690    1          #  position angle (PA) [deg: Up=0, Left=90]
F1) 0.0001   0.0000   1 1  #  azim. Fourier mode 1, amplitude, & phase angle
F3) 0.0001   0.0000   1 1  #  azim. Fourier mode 3, amplitude, & phase angle
 Z) 0                      #  output option (0 = resid., 1 = Don't subtract)

# Object number: 3
 0) expdisk                #  object type
 1) 48.5180  51.2800  1 1  #  position x, y
 3) 20.0890     1          #  integrated magnitude
 4) 5.1160      1          #  R_s (disk scale-length)   [pix]
 9) 0.7570      1          #  axis ratio (b/a)
10) -60.3690    1          #  position angle (PA) [deg: Up=0, Left=90]
C0) -0.05       0          #  diskyness(-)/boxyness(+)
 Z) 0                      #  output option (0 = resid., 1 = Don't subtract)
```

Figure 27. Example Galfit input file[20].

7 Refrences

References

[1] Kormendy J., Ho L. C., , ARA&A, 51, 511 (2013)

[2] Mo, H., van den Bosch, F.˜C., & White, S., Galaxy Formation and Evolution, by Houjun Mo , Frank van den Bosch , Simon White, Cambridge, UK: Cambridge University Press, (2010)

[3] Sersic JL. . Atlas de Galaxias Australes. Cordoba: Obs. Astron. Univ. Nacional de Cordoba (1968)

[4] Graham A. W., Scott N., 2015, ApJ, 798, 54(2015)

[5] Yang G., Brandt W.˜N., Alexander D.˜M., Chen C.-T.˜J., Ni Q., Vito F., Zhu F.-F., MNRAS, 485, 3721 (2019)

[6] Magorrian, J., et al., AJ, 115, 2285 (1998)

[7] Gebhardt K., et al., 2000, ApJ, 539, L13(2000)

[8] Häaring N., Rix H.-W., 2004, ApJ, 604, L89 (2004)

[9] Ferrarese L., Merritt D., ApJ, 539, L9 (2000)

[10] Ferrarese, L., ApJ, 578, 90 (2002)

[11] Kormendy, J., & Richstone, D., ARA&A, 33, 581 (1995)

[12] Silk, J.,& Rees, M. J. , A&A, 331, L1 (1998)

[13] Läsker, R., Ferrarese, L., & van de Ven, G. , ApJ, 780, 69 (2014a)

[14] Vika, M., et al. , MNRAS, 419, 2264 (2012)

[15] Läsker, R., et al. , ApJ, 825, 3 (2016)

[16] van Son, L.˜A.˜C., Barber, C., Bahé, Y.˜M., et al. mnras, 485, 396. (2019)

[17] van den Bosch, R. C. E. , ApJ, 831, 134 (2016)

[18] Nilson P., 1973, Uppsala general catalogue of galaxies. Uppsala Astron. Obs

[19] Peng, C.˜Y., Ho, L.˜C., Impey, C.˜D., et al. , aj, 124, 266. (2002)

[20] Peng, C.˜Y., Ph.D. Thesis, 4623 (2004)

[21] Busch, G. 2016, arXiv e-prints, arXiv:1611.07872

[22] Dressler, A., & Richstone, D. O. 1988, ApJ, 324, 701, doi: 10.1086/165930

[23] Läsker, R., Ferrarese, L., van de Ven, G., & Shankar, F. , ApJ, 780, 70 (2014b)

[24] Nelson, C. H., Green, R. F., Bower, G., Gebhardt, K., & Weistrop, D. 2004, ApJ, 615, 652

[25] Kim, M., Ho, L. C., Peng, C. Y., et al. 2008, ApJ, 687, 767

[26] Jiang, Y.-F., & Goodman, J. 2011, ApJ, 730, 45

[27] Davari, R., Ho, L.˜C., Peng, C.˜Y., et al., , 787, 69.(2014)

[28] dos Reis, S.˜N., Buitrago, F., Papaderos, P., et al., , 634, A11. (2020)

[29] Jiang, Y.F., Greene, J.E., & Ho, L.C. 2011, apjl, 737, L45.(2011)

[30] van der Wel, A., Bell, E.˜F., Häussler, B., et al., , 203, 24.(2012)

[31] Tuccillo, D., Huertas-Company, M., Decencière, E., et al., , 475, 894.(2018)

[32] Häussler, B., McIntosh, D.˜H., Barden, M., et al. 2007, , 172, 615.(2007)

[33] McConnell N. J., Ma C.-P., 2013, ApJ, 764, 184